



Review

Enhanced Performance of Silicon Negative Electrodes Compositing with Titanium Carbide Based MXenes for Lithium-Ion Batteries

Tingting Jiang ¹ , Hao Yang ¹ and George Zheng Chen ^{1,2,*}

¹ The State Key Laboratory of Refractories and Metallurgy, College of Materials and Metallurgy, Wuhan University of Science and Technology, Wuhan 430081, China; ttjiang@wust.edu.cn (T.J.); haoyang@wust.edu.cn (H.Y.)

² Department of Chemical and Environmental Engineering, Faculty of Engineering, University of Nottingham, Nottingham NG2 7RD, UK

* Correspondence: george.chen@nottingham.ac.uk

Abstract: Silicon is considered as one of the most promising candidates for the next generation negative electrode (negatrode) materials in lithium-ion batteries (LIBs) due to its high theoretical specific capacity, appropriate lithiation potential range, and fairly abundant resources. However, the practical application of silicon negatrodes is hampered by the poor cycling and rate performances resulting mainly from the huge volume change during Li⁺ insertion/extraction. Various composite structures have been investigated to maintain the structural integrity and improve the stability and electric conductivity of silicon-based negatrodes. Of these, 2D transition-metal carbides, also known as MXenes (e.g., Ti₃C₂T_x), have become increasingly attractive for energy storage applications because of their excellent electric, electrochemical and mechanical properties and potential uses as the matrix for construction of 3D networks with larger buffering spaces and more effective charge carrier conduction in silicon-based negatrodes. This article reviews specifically composite negatrodes of silicon with titanium-carbide-based MXenes for LIBs from the materials perspective. The structures design, preparation method, interface control, and their effects on electrochemical performances are comprehensively elaborated on. It is shown that the recent development of Si/MXene-based negatrodes presents great potential for future applications.

Keywords: Si-based composites; MXenes; negatrode materials; electrochemical performance



Citation: Jiang, T.; Yang, H.; Chen, G.Z. Enhanced Performance of Silicon Negative Electrodes Compositing with Titanium Carbide Based MXenes for Lithium-Ion Batteries. *Nanoenergy Adv.* **2022**, *2*, 165–196. <https://doi.org/10.3390/nanoenergyadv2020007>

Academic Editors: Peter D. Lund, Imran Asghar and Ya Yang

Received: 13 January 2022

Accepted: 30 March 2022

Published: 1 April 2022

Publisher's Note: MDPI stays neutral with regard to jurisdictional claims in published maps and institutional affiliations.



Copyright: © 2022 by the authors. Licensee MDPI, Basel, Switzerland. This article is an open access article distributed under the terms and conditions of the Creative Commons Attribution (CC BY) license (<https://creativecommons.org/licenses/by/4.0/>).

1. Introduction

1.1. Silicon Based Negative Electrode Materials for LIBs

Various forms of clean energy from renewable sources, e.g., wind and sunlight, are increasingly being utilized, which should more effectively sustain energy supply and reduce carbon emission. However, the discontinuity and geographic restrictions on renewable energy call for affordable and effective storage technologies. Electrochemical energy storage (EES) devices could help store and deliver the energy from wind turbines and solar panels into the power grid [1]. Lithium-ion batteries (LIBs) have been used in portable electric devices and electric vehicles (EVs) for years due to their high energy and power densities, satisfactory cycle life and the affordable materials and manufacturing costs. To meet the growing market demand for cheaper and more efficient energy storage technologies for EVs and power grids, higher energy storage density and efficiency, and a longer cycle life should be achieved in the next generation of LIBs [2].

Silicon (Si) is considered as one of the most promising candidates for next generation negative electrode (negatrode) materials in LIBs due to its much higher theoretical specific charge capacity than the current commercial negatrode (carbon-based). With its abundant resources and reasonable conductivity in a doped state, Si can also offer an appropriate

lithiation potential range (0.1 V vs. Li^+/Li) [3]. However, due to the large volume change during lithiation and delithiation, cracking, pulverization and subsequent exfoliation from the current collector may lead to irreversible capacity loss in Si-based active materials [4]. As shown in Figure 1a, after lithiation, particles of a large size would crack and pulverization may occur after many cycles. Even though nanoparticles that would not crack can be used, volume change may also lead to electrical isolation for silicon. The increased formation of new surfaces from silicon cracking and pulverization may cause repeated breakage and a formation of the solid electrolyte interface (SEI) layer, leading to the continuous consumption of Li^+ ion in the electrolyte [5]. Moreover, as a typical semiconductor, the electronic conductivity of silicon is not ideal for discharging and charging, resulting in poor performance rates.

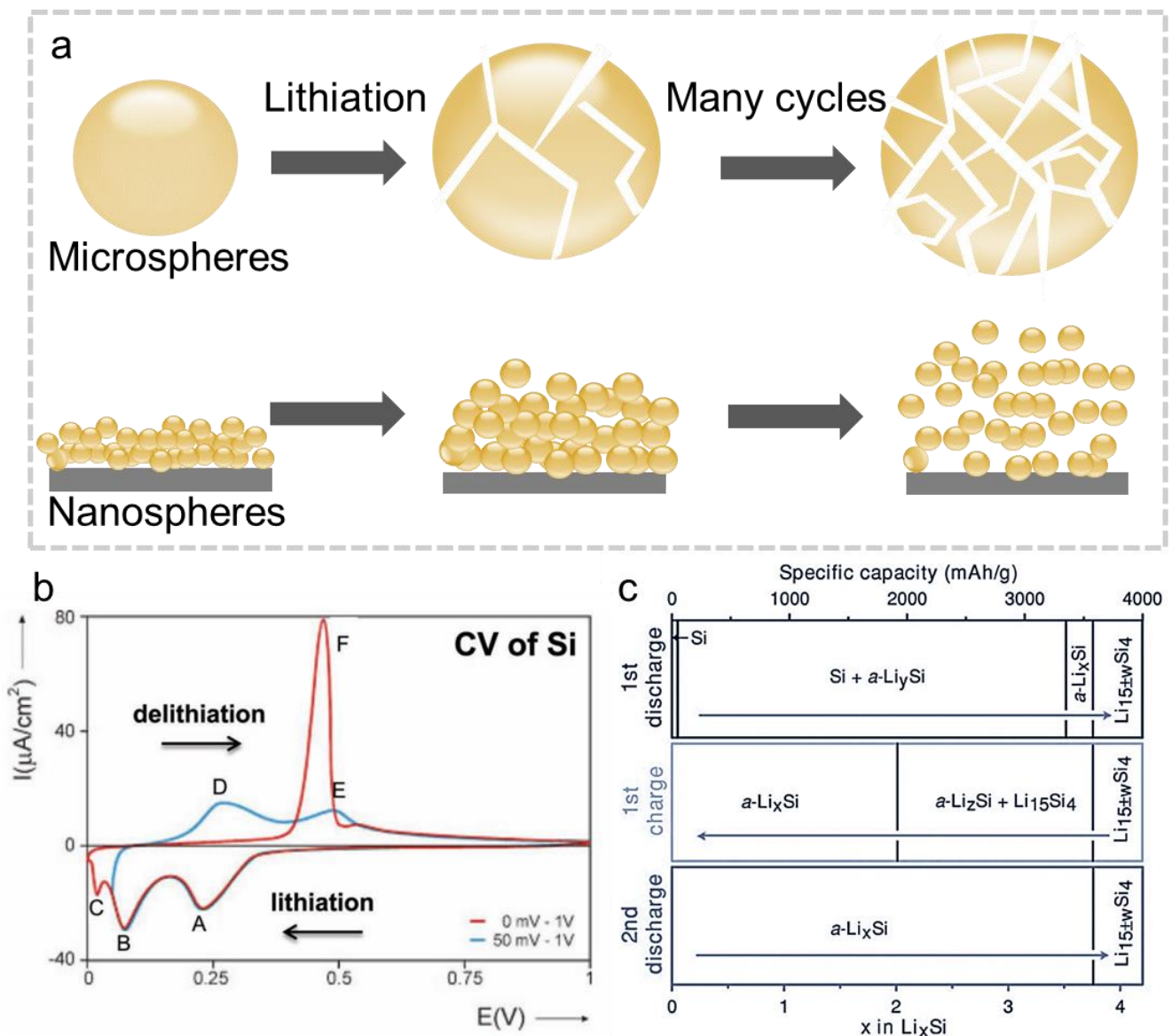
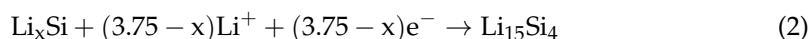


Figure 1. (a) Schematic illustration of the failure mechanism during the electrochemical cycling of a silicon negatrod. (b) Typical Cyclic voltammogram (CV) of Si. (c) Phase diagrams at different stages of the charge–discharge cycling of a Li/Si negatrod between 0.005 and 0.9 V at room temperature. (Reprinted with permission from Ref. [6], Copyright 2012 John Wiley and Sons. Reprinted with permission from Ref. [7], Copyright 2007 John Wiley and Sons).

A typical CV for Si is displayed in Figure 1b [6]. The broad lithiation peaks A and B indicate the transformation from crystalline silicon to an amorphous Li-Si alloy, and the sharp peak C refers to the crystallization of α -Li_xSi. The delithiation peak F corresponds to the reverse process. In the lithiation process, silicon experiences a series of phase transformations. As the potential becomes more negative, crystalline silicon firstly transforms to an amorphous phase and remains in the amorphous state at higher Li/Si ratios via the reactions below.



The stoichiometry of Li₁₅Si₄ may be achieved when the potential is as low as 50 mV vs. Li⁺/Li, accompanied by a volume expansion of as much as 400% [8,9]. During delithiation, no crystalline Si form again, indicating that the crystalline Li₁₅Si₄ (Li_{3.75}Si) phase is delithiated to form an amorphous Li_xSi phase according to the following reaction.



Figure 1c exhibits a phase diagram of silicon negatrod during charge–discharge cycling between 0.005 and 0.900 V at room temperature [7].

Various effective strategies have been developed to overcome these drawbacks and to promote the probable application of silicon negatrod in LIBs. Constructing nanostructures could restrain pulverization, thanks to the reduced transport lengths of electrons and Li⁺ ions and a consequently larger tolerance to volume change as well as an increase in the contact area between the active material and electrolyte [10,11]. On the other hand, compositing with other materials with higher conductivity and mechanical stability could help to maintain the structure of silicon as well as promote carrier transport in the active materials. For example, it was observed that coating a layer of carbon [12–14], SiO_x [15–17], metal, and metal oxide [18–20] on silicon nanomaterials could suppress the volume expansion of silicon and buffer the stress, thereby promoting better electrochemical performance and structural stability.

1.2. Silicon/2D Material Composites

In two dimensional (2D) materials, the high specific surface area and stable mechanical properties offer more ion insertion channels and lead to fast ion transport. For example, graphene [21], phosphorene [22], borophene [23], MoS₂ [24], Ti₃C₂T_x [25] and V₂O₅ [26] have been widely investigated as electrodes or as part of electrodes for LIB applications. Such flexible 2D-layered materials could coat silicon to buffer the volume change during lithiation and delithiation so as to increase the cycle life, while the large specific surface area and high conductivity could increase the high-rate capacity. Among these 2D materials, graphene is most commonly used to form various composite structures with silicon, achieving excellent performance [27–29].

Graphenes are usually used based on their physical properties, e.g., high conductivity for electrons, high surface area for loading and dispersion of active materials, and structure modification. However, unlike graphenes, MXenes are advantageous in their rich composition and surface chemistry, surface hydrophilicity, and energy or lithium storage capacities. Particularly, titanium carbide MXene (Ti₃C₂T_x) has been most intensively studied and can be used as the lithium host material for LIBs due to its considerable theoretical capacity (320 mAh g⁻¹), lower Li⁺ diffusion barrier (0.07 eV) compared to that of graphene (0.3 eV), moderate potential ranges vs. Li⁺/Li, and low cost. Therefore, in this review, titanium carbide MXene and its various composites with silicon are mainly discussed.

1.3. Application of MXenes in LIBs

MXenes, consisting of layered transition metal carbides, nitrides, and carbonitrides, are a recently emergent family of 2D nanomaterials. By selectively etching the layer-structured MAX phase materials which consist of transition metal (M, e.g., Ti, Zr, Cr) and A group

elements (A, e.g., Al, Si, Ga, Ge), and carbon or nitrogen (X), MXenes can be prepared with a general formula of $M_{n+1}X_nT_x$ ($n = 1$ to 3), where T refers to the terminal functional groups [30]. Due to the large layer spacing, good conductivity, low diffusion barrier, highly negative working potentials, unique 2D morphology, excellent mechanical properties, and environmental friendliness, MXenes have shown their potential as electrode materials in EES devices including LIBs [31] and supercapacitors [32]. Besides, MXenes have proven applications in electromagnetic interference shielding [33], oxygen evolution reactions [34], electrochemical sensors [35], and silicon-based solar cells [36]. More specifically, $Ti_3C_2T_x$ is one of the most representative MXene materials applicable as negatrod materials in LIBs [37]. Although MXenes only have a Li storage capacity similar to that of commercial graphite electrodes, their mechanical stability, conductivity, and ion transportation properties can lead to long cycling durability and high rate capability [38]. Therefore, MXenes can be used as a coating layer or matrix to composite with other electrode materials of high theoretical Li storage capacity. For instance, Ahmed et al. [39] prepared HfO_2 -coated SnO_2 /MXene electrodes by depositing SnO_2 on MXene terminated with oxygen, fluorine, and hydroxyl groups with atomic layer deposition and demonstrated good electrochemical performance with a stable capacity of 843 mAh g^{-1} . In the same year, Chen et al. [40] synthesized 2D MoS_2 -on-MXene heterostructures via in situ sulfidation of $Mo_2Ti_3C_2T_x$ MXene with improved and stable Li storage performance. Furthermore, as the main focus of this review, MXenes show a good flexibility and the capability to composite with silicon for improved performance. For example, the $Si@Ti_3C_2$ composites [41] can retain 60~70% of the weight to achieve 300 mAh g^{-1} which is the specific capacity of commercial graphite negatrod material. Similar volumetric performance parameters are expected because MXenes have a comparable density with graphite.

It should be pointed out that silicon has also been composited with carbon materials to achieve improved performances. In Si/carbon coating composites, the amorphous carbon layer could accommodate the volume change in silicon and improve the overall electroconductivity of composite particles. The preparation method is usually facile to mass manufacture. However, the aggregation and collapse of the Si/carbon structure could not be mitigated completely. Graphene exhibits excellent electrical, mechanical, and thermal properties and has been widely used to form Si/graphene composites, which have a more stable structure and higher carrier transportation rate. The preparation process is more complicated partly because of the high aggregation tendency of graphene sheets, and are therefore more expensive than that of the Si/carbon. Si/MXene composites exhibit similar advantages as that of Si/graphene, but the bonding of Si with MXene is generally more stable due to the various surface functional groups and because MXenes express a lower Li^+ diffusion barrier than graphene.

Since Si/MXene composites have only been studied in recent years, they are far from being fully explored. At present, questions as to whether MXenes may replace graphene for compositing with Si, or solve all problems of the Si negatrod, or whether they could be commercially implemented still remain unanswered. However, past research has shown that Si/MXenes, particularly those based on titanium carbides, possess unique and desirable properties with relevance to LIBs. In this review, silicon/titanium carbide-based MXenes composites, as negatrod materials for LIBs, are reviewed from the materials perspective. The second section presents the structure design, preparation methods and interface control of Si/MXene-based negatrod materials. The third section is concerned with the effects of composite construction on electrochemical performances. Finally, a summary and critique of the literature findings will be provided. The implication of these findings for future research into Si/MXene-based negatrod materials for LIBs will also be discussed.

2. Structures and Preparation Strategies of Si/MXene Composites as Negatrod Materials in LIBs

As a typical MXene material, $Ti_3C_2T_x$ can be achieved by etching the layered ternary MAX phases and presents a 2D configuration with a series of terminal functional groups

such as -F, -O, and -OH [42]. The Ti-C bond in the MXene helps to maintain the stable layered structure. In 2011, Gogotsi et al. published a report on 2D nanosheets, composed of a few Ti_3C_2 layers and conical scrolls constructed by in situ exfoliation of Ti_3AlC_2 in hydrofluoric acid [43]. These 2D nanosheets were then called MXene with an accordion-like structure. In their work, there are interspaces of about dozens to several hundred nanometers between the nanosheets. Then, in the following works, researchers also prepared single and few-layered Ti_3C_2 nanosheets which are highly dispersible in water once Al layers are removed using the mixture of LiF and HCl. Therefore, Si/MXene composites can be synthesized with the above two kinds of MXenes. These composites can be categorized into several structures, such as self-standing film and layer-by-layer, three-dimensional (3D), and coating structures. These different structures of Si/MXene composites are illustrated in Figure 2. In this section, different composite structures, their advantages and relevant synthesis methods, and the interface control in these structures will be discussed.

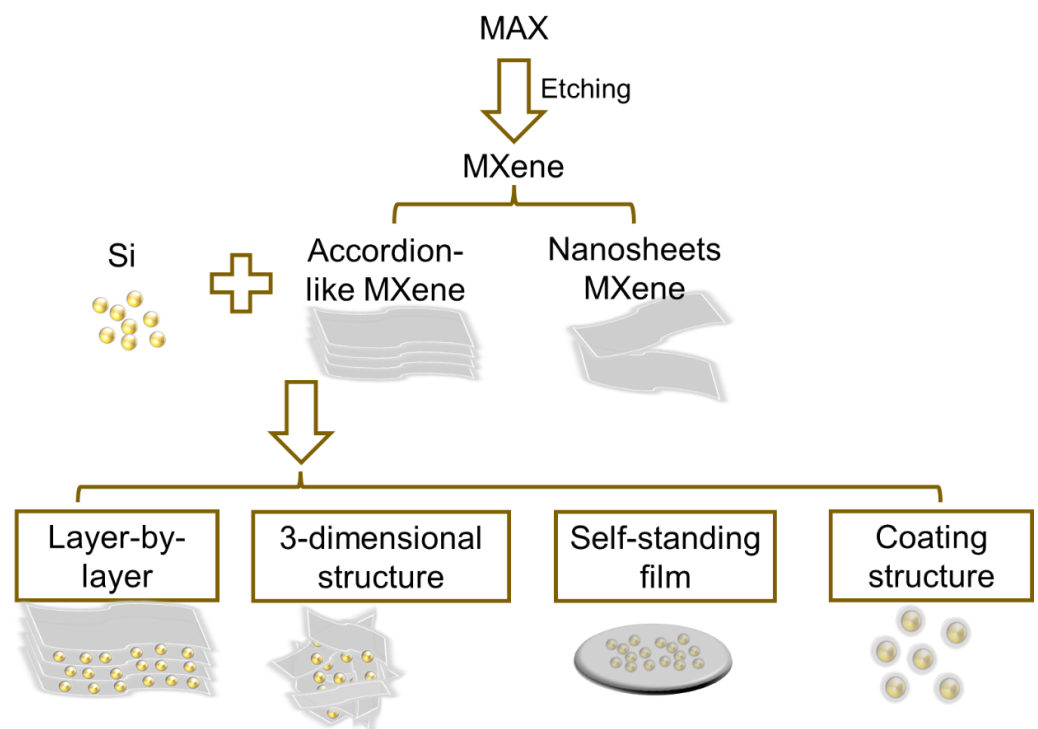


Figure 2. Schematic of the syntheses of Si/MXene composites with different structures.

2.1. Structures of Si/MXene Composites

2.1.1. Layer-by-Layer Structure

As mentioned above, the commercialization of silicon-based negatodes is limited mainly by the inherently low electron and Li^+ ion conductivities but more importantly by the huge volume change during repeated lithiation and delithiation processes, which may then lead to fractures in the active material, and a loss of contact with the electrode. Nanoparticles are often used to prevent pulverization and to increase the contacting area with electrolytes [44]. By combining silicon nanoparticles (SiNPs) with both accordion-like and thin nanosheets MXenes, layer-by-layer structured composites can be achieved, which is the most investigated structure so far [45,46].

After the exfoliation of the Al layer of the respective MAX phase material, the resulting MXene exhibits a loosely packed accordion-like structure composed of multiple layers with the interlayer space between the nanosheets being large enough for the intercalation of SiNPs. As for the thin MXene nanosheets, layer-by-layer self-assembly through electrostatic interactions between SiNPs and MXenes can be achieved in solution. This layer-by-layer structure mainly benefits from the following advantages. (1) The loose layered structure of

MXene can accommodate SiNPs via the electrostatic effect due to the terminal functional groups of MXene, which can restrict volume expansion and prevent the aggregation of SiNPs during lithiation and delithiation. (2) The excellent electrical properties as well as the direct electronic transport pathway of layered MXene can effectively promote carrier transfer and hence improve the rate performance. (3) The satisfactory mechanical properties of MXene nanosheets can help to maintain the stability and integrity of the whole composite structure, while the large specific surface area can increase the reaction interface between active material and electrolyte.

The first Si/MXene composites with a layer-by-layer structure were reported in 2018 [47], after the simple mixing of SiNPs and the accordion-like MXenes. Figure 3a–c show an illustration (Figure 3a) of the typical structure of accordion-like Ti_3C_2 MXene in accordance with SEM observations (Figure 3b,c). SiNPs were deposited on the surfaces of Ti_3C_2 layers, and inserted into the space between nanosheets. Although nanoparticles still exhibited aggregation, the layered structure of MXene alleviated the issue. The XRD patterns (Figure 3d) demonstrated the successful synthesis of this layer-by-layer Si@ Ti_3C_2 composite.

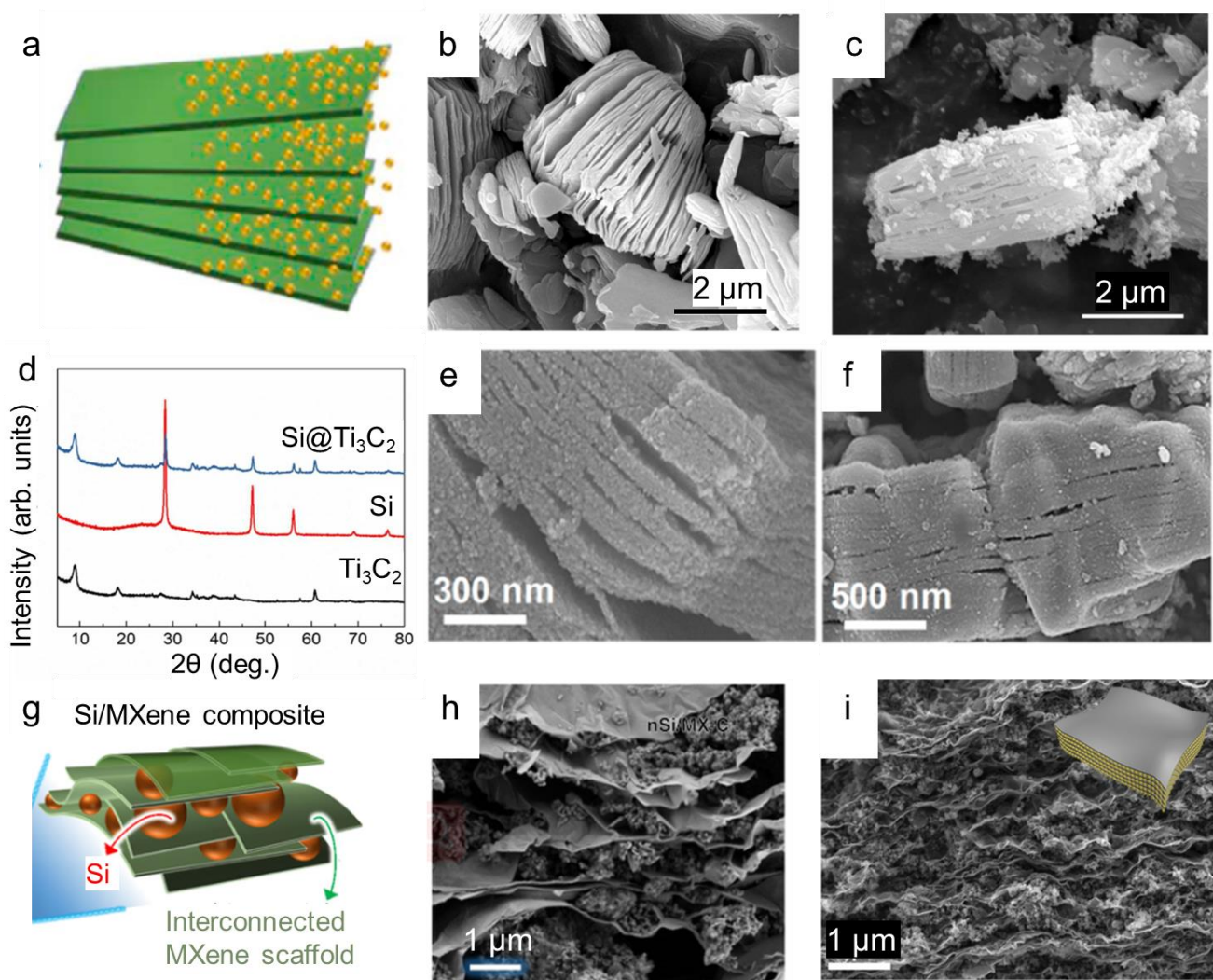


Figure 3. Layer-by-layer structured Si/MXene nanocomposites. (a) Schematic illustration of Si/ Ti_3C_2 . SEM images of (b) Ti_3C_2 and (c) Si/ Ti_3C_2 . (d) XRD patterns of Si, Ti_3C_2 , and Si/ Ti_3C_2 . SEM images of (e) MXene/Si and (f) MXene/Si@ SiO_x @C-2. (Reprinted with permission from Ref. [47], Copyright 2018 Elsevier; reprinted with permission from Ref. [48], Copyright 2019 ACS Publishers, respectively).

(g) Schematic illustration, and (h) cross-sectional SEM image of the nSi/MXene-C electrode. (i) The cross-section FESEM image (schematic in the inset) of Si/Ti₃C₂ superstructures. (Reprinted with permission from Ref. [49], Copyright 2019 Springer Nature; reprinted with permission from Ref. [50], Copyright 2020 Elsevier, respectively).

Zhang et al. also prepared an MXene/Si@SiO_x@C layer-by-layer assembling superstructure with accordion-like MXene [48]. The SiO_x layer was first deposited on MXene sheets using the Stöber method and then magnesiothermic reduction to the Si/MXene composite was performed, followed by the carbonization process. In Figure 3e,f, SiNPs were uniformly distributed on the surface of the MXene nanoflakes and the thin SiO_x and carbon layers were coated on the outside of MXene/Si.

The dispersed few-layered nanosheets of MXene can also be used to construct the layer-by-layer structure [49]. As shown in Figure 3g, by casting the slurry of MXene nanosheets, MXene nanoflakes interconnected and stacked into a thin film with SiNPs caught in the space between nanoflakes. Figure 3h shows the layer-by-layer morphology of this composite, in which SiNPs were anchored on MXenes. In 2020, Yang et al. [50] also reported a similar structure of Si/MXene. Derived from etching the MAX phase precursor by a mixed LiF and HCl solution, thin few-layered MXene nanosheets and the treated SiNPs formed the layer-by-layer structure (Figure 3i) through electrostatic self-assembly are also presented.

In addition, there were some attempts to surface-modify or add a third component to achieve a more controllable layer-by-layer structure [41,45,51]. The layer-by-layer Si/MXene structure integrates all the merits of both silicon and MXene, and is suitable and promising for the large-scale application of silicon-based negatodes.

2.1.2. Self-Standing Film

Apart from the layer-by-layer structure, the thin few-layered MXene nanosheets can form free-standing films due to their unique bonding and mechanical properties. By mixing with MXene, SiNPs can be fixed inside the free-standing film supported by MXene nanosheets. The microstructure of this free-standing film prepared by vacuum filtration is quite similar to that of the layer-by-layer Si/MXene composites, but can be directly used as binder-free electrodes in LIBs [52,53].

This free-standing film of Si/MXene composites could provide a pathway to foster the large-scale application of silicon-based negatodes in LIBs, benefiting from several advantages, as follows. (1) The 3D flexible and free-standing structure consisting of covalently anchored silicon on MXene nanosheets can effectively confine the volume change of silicon during lithiation/delithiation. (2) The highly conductive MXene can act as a matrix, the binder instead of inactive binders such as polyvinylidene fluoride (PVDF) and sodium carboxymethyl cellulose (CMC), and as well as the current collector, which can increase the active material ratio and facilitate carrier transport during dis-/charging.

Figure 4a illustrates the structure of the Si/MXene free-standing film, which is flexible, layer-by-layer, free-standing, and paper-like. Tian et al. prepared this film by vacuum filtration [54]. The cross-sectional SEM image of this Si/MXene free-standing film in Figure 4b shows that SiNPs were distributed between the thin MXene flakes, which were large, flexible, and freestanding. Li et al. [52] performed a similar filtration process and achieved a free-standing film in which MXenes acted as matrix for loading silicon.

At the same time, Zhang et al. composited Si@C particles with MXene, which could be used directly on electrodes for LIBs [53]. The images in Figure 4d show its appearance and flexibility, and it sustained the integrity and stability when bending, rolling, twisting, folding, and folding into a windmill. From cross-sectional SEM images (Figure 4e,f), it can be seen that this MXene-bonded Si@C film electrode presents a porous 3D layered structure with a thickness of about 10 μm, in which the Si@C nanoparticles are embedded in the MXene framework.

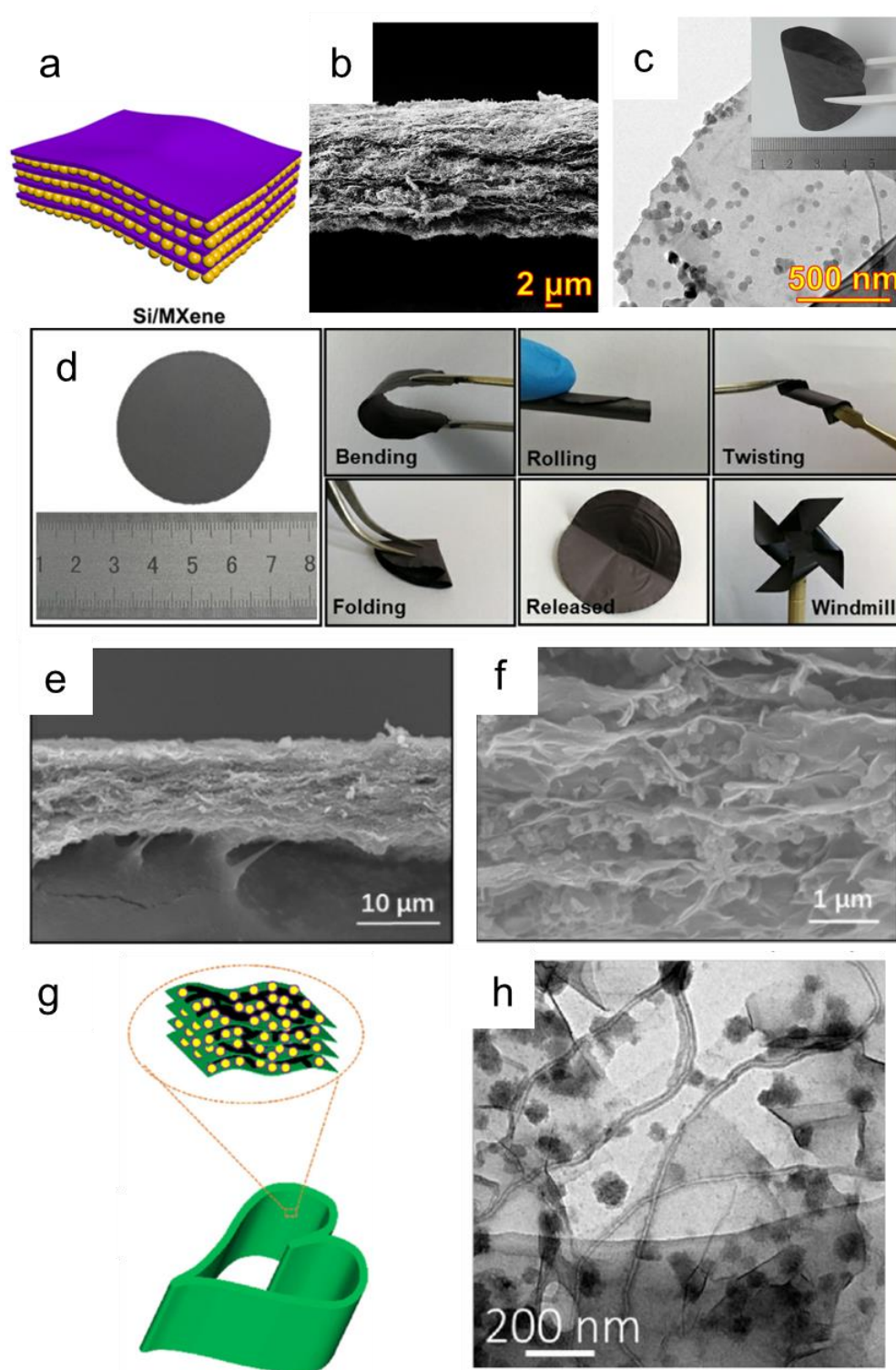


Figure 4. Self-standing films of Si/MXene composites. (a) Schematic illustration, (b) the cross-sectional SEM image, and (c) the TEM images of the Si/MXene free-standing film (inset photograph). (d) The appearance and flexibility and cross-sectional SEM images of the MXene-bonded Si@C free-standing film at (e) low- and (f) high-magnifications. (g) Schematic illustration and (h) HRTEM image of the $\text{Ti}_3\text{C}_2\text{T}_x\text{-CNT/SiNPs}$ film. (Reprinted with permission from Ref. [54], Copyright 2019 ACS Publishers; reprinted with permission from Ref. [53], Copyright 2020 John Wiley and Sons; reprinted with permission from Ref. [55], Copyright 2020 Elsevier, respectively).

The free-standing film can also be prepared by combining silicon, MXene, and one-dimensional carbon nanotubes (CNTs). In 2020, Cao et al. [55] prepared flexible free-standing and resilient $\text{Ti}_3\text{C}_2\text{T}_x$ -CNT/SiNPs films with a hierarchical porous structure (Figure 4g) by vacuum filtration by means of electrostatic interactions. In TEM images (Figure 4h), the SiNPs, which were anchored tightly to the thin MXene plate, and the interconnected CNTs were distributed uniformly and formed a network, preventing the aggregation of silicon.

By eliminating the typical binder, conductive agent, and copper current collector, the Si/MXene free-standing film could provide a higher specific capacity and power density at a relatively lower cost. Preparation of the large-area uniform film is the key point of their application in mass production.

2.1.3. Three-Dimensional Structure

The three-dimensional (3D) porous structure has been investigated thoroughly in Si/graphene composites. With a similar 2D structure and morphology to graphene, MXene could also be constructed into a 3D matrix to allow SiNPs to form the porous structure. Both accordion-like and thin single- or few-layered MXene nanosheets can be designed and fabricated into a 3D structure with silicon [56,57].

Similarly to Si/MXene composites, the 3D porous Si/MXene attracted much attention because of the following reasons. (1) In the 3D Si/MXene porous structure, MXene nanosheets can interconnect into a skeleton-like frame, with SiNPs inside the skeleton by bonding and adherent to MXene plate. (2) The good mechanical strength of MXenes helps to alleviate the impact of volume expansion of Si during cycling and stabilize the 3D structure. (3) The porous structure could provide conductive pathways and a larger specific surface area for more active reaction sites. This 3D porous structure can be achieved by for example mechanical mixing and freeze-drying.

Wang et al. [58] performed a freeze-drying process in liquid nitrogen with the suspension mixture of Si and few-layered MXene nanosheets and prepared $\text{Si}@\text{Ti}_3\text{C}_2\text{T}_x$ composite with a 3D structure, as shown in Figure 5a. After etching and ultrasonically delaminating, $\text{Ti}_3\text{C}_2\text{T}_x$ (Figure 5b) nanosheets with a two-dimensional morphology could be obtained which were then mixed with SiNPs with a diameter of about 50 nm. After freeze-drying, the few-layered $\text{Ti}_3\text{C}_2\text{T}_x$ nanosheets presented a wrinkled and curled morphology, where SiNPs wrapped inside the space and anchored on the nanosheets (Figure 5c).

Since MXene could act as both the matrix of 3D structures and silicon loader, Li et al. [59] designed 3D hierarchical and porous structures in Si/MXene composites with dual MXene protection ($\text{SiNP}@\text{MXene1}/\text{MXene2}$). This dual MXene structure is shown schematically in Figure 5d. Firstly, the few-layered MXene sheets interacted with CTAB (cetyltrimethylammonium bromide)-treated SiNPs via electrostatic self-assembly, leading to Si particles being riveted to MXene plates ($\text{SiNP}@\text{MXene1}$). Then, this $\text{SiNP}@\text{MXene1}$ precursor was embedded into another 3D MXene matrix by the hydrothermal process, followed by freeze-drying. The prepared composites showed a particle size of 1 to 2 μm , and the SEM micromorphology is displayed in Figure 5e,f. The cross-linked MXene nanosheets provided a skeleton of a 3D porous structure in which $\text{SiNP}@\text{MXene1}$ composite nanoparticles were embedded. In this dual MXene structure, the internal MXene1 was present, which was coated on SiNPs to restrict volume expansion and prevent aggregation. The external MXene2 skeleton supported the 3D structure with abundant channels for electrolyte permeation and buffering volume changes. The MXene1 coating layer also helped to form a more stable SEI film.

Introducing another component, e.g., carbon, into the 3D porous composites could further improve the structural stability and hence the cycling capacity. In 2019, Liu et al. [60] reported a dual-bond restricted MXene-Si-CNT composite as a negative material with enhanced electrochemical performance. By ball-milling MXene nanosheets, Si, and CNTs, the 3D porous homogeneous MXene/Si/CNTs composites were obtained. The energy from ball-milling reinforced the combination of the three reagents into a composite via the formation of the Ti-Si and C-Si bonds. Figure 5g,h illustrate the structure and micro-

morphology of this composite, revealing a multidimensionally constructed architecture in which MXene and Si particles were grounded together and CNTs twined around the MXene-Si aggregates. Moreover, the SiNPs were uniformly attached to the surfaces of individual MXene plates.

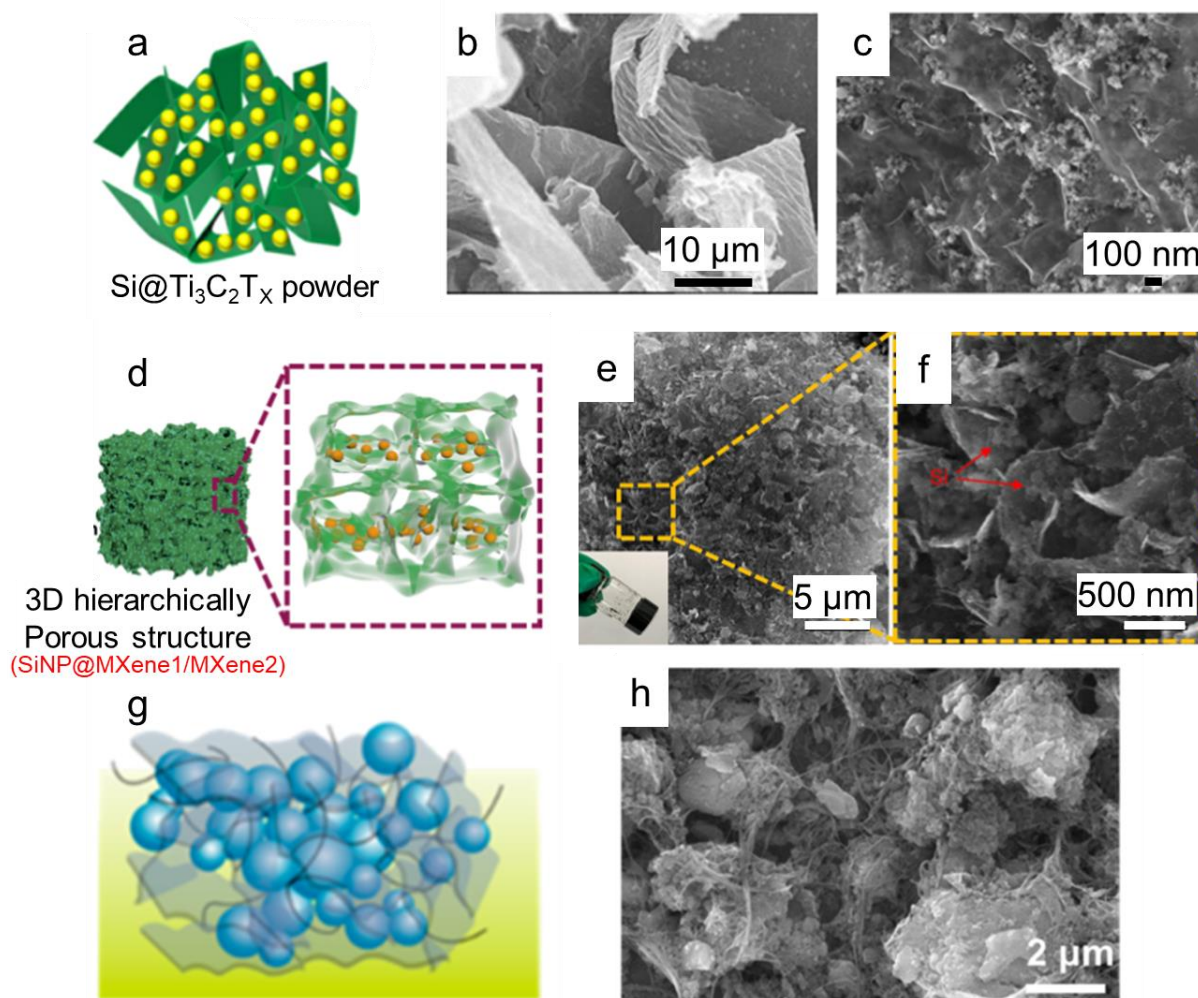


Figure 5. 3D structure of Si/MXene composites. (a) Schematic of the $\text{Si@Ti}_3\text{C}_2\text{T}_x$ nanocomposite. SEM image of (b) $\text{Ti}_3\text{C}_2\text{T}_x$ and (c) $\text{Si@Ti}_3\text{C}_2\text{T}_x$ nanocomposite. (Reprinted with permission from Ref. [58], Copyright 2021 Elsevier). (d) Schematic diagram and (e,f) SEM images of $\text{SiNP@MXene1/MXene2}$. (g) Illustration and (h) SEM images of ball-milled MSC composites. (Reprinted with permission from Ref. [59], Copyright 2020 ACS Publishers. Reprinted with permission from Ref. [60], Copyright 2019 ACS Publishers).

In addition to those mentioned above, other 3D Si-based composites were reported. For example, uniformly dispersed Si nanospheres [56] or $\text{Si/SiO}_x\text{@TiO}_2$ nano aggregates [61] were deposited on thin MXene nanosheets. The Si/MXene/CNTs composites were also prepared by electrospinning and pyrolysis into fibrous structures, which finally turned into 3D structures with crosslinked fibers [62]. Meng et al. [63] rolled up MXene nanosheets into scrolls and added SiNPs simultaneously. The $\text{Ti}_3\text{C}_2\text{T}_x$ was rolled into hollow and fully curled scrolls with Si particles inside, and then the scrolls interconnected with each other into a 3D porous structure.

The 3D porous structure of Si/MXene composites is diverse. However, the connection and synergistic effect between the components are of great importance and should be thoroughly considered according to the synthetic process and electrochemical performances.

2.1.4. Coating Structure

Coating is one of the most frequently used strategies for surface modification and in the formation of silicon composites. The coating can be amorphous or crystalline, and may comprise amorphous carbon, metal oxide, metal, graphene and CNTs. As a flexible 2D material, single- or few-layered MXene nanosheets can be coated thinly on silicon, forming core-shell or overall coating structures.

Similar to the other three structures discussed above, a MXene coating could also function as a robust and flexible layer to accommodate for the volume expansion of silicon to prevent the pulverization. The bonds between silicon and $\text{Ti}_3\text{C}_2\text{T}_x$ or other highly conductive MXene are beneficial to electron transport. In such structures, the most important point is that wrapping silicon with a homogeneous MXene layer can effectively prevent nanoparticles from directly contacting the electrolyte and thus enable the formation of a stable SEI film (in some cases, the artificial SEI film will form). Then, the interfacial stability and subsequently the cycling stability can be improved.

Figure 6a shows the structure of the MXene coating on a porous silicon sphere prepared by Xia et al. in 2020 [64]. With the help of surface groups of MXene nanosheets, porous silicon nanospheres were closely wrapped by MXene nanosheets following the interfacial assembly strategy. Figure 6b–d show the SEM, TEM, and HRTEM images of these Si@MXene composites, respectively. Each Si nanosphere is tightly wrapped by the thin, wrinkled MXene layer, forming the core-shell structure. The Si sphere has a diameter of around 500 nm, while the shell layer is about 5 nm thick. In the HRTEM image, the lattice planes of both Si and MXene are clearly visible.

Besides the core-shell structure, Yan et al. prepared another coating structure, in which a bundle of SiNPs were encapsulated in robust micrometer-sized MXene frameworks, as shown in Figure 6e. According to Figure 6f, micrometer-sized Si@MXene capsules are mainly spherical with a diameter of several micrometers. It can be seen in Figure 6g,h that SiNPs are dispersed uniformly between the MXene nanosheets shell and there are voids inside the capsule which could provide space for the volume expansion of silicon.

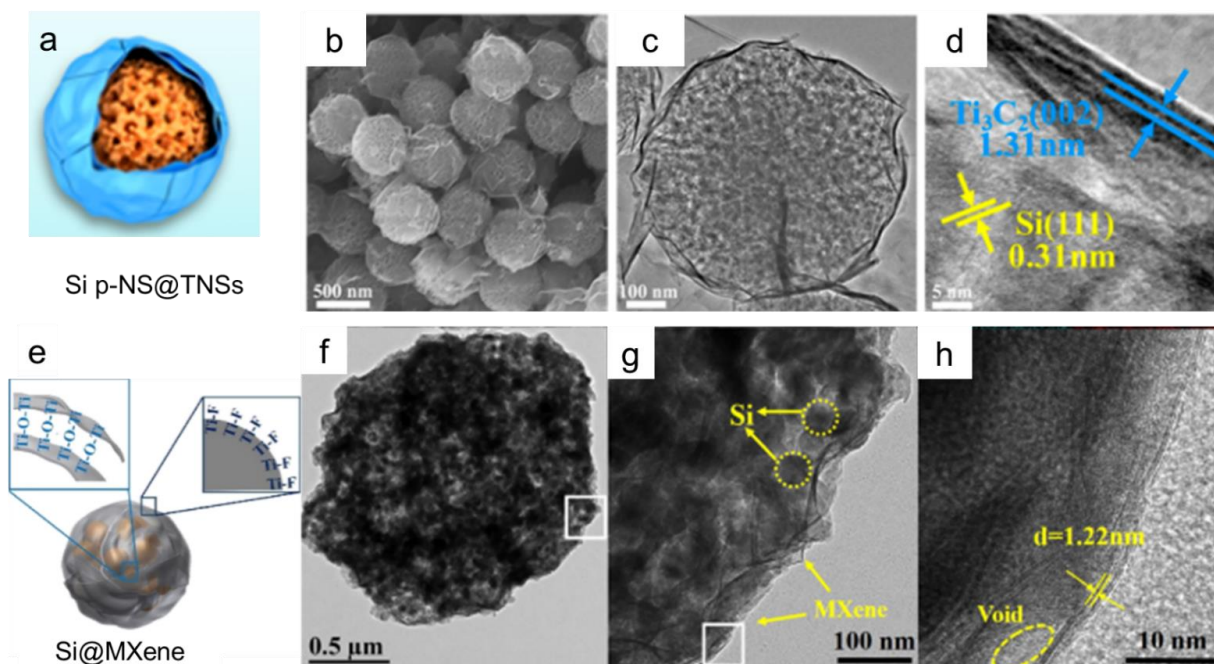


Figure 6. Coating structures of Si/MXene composites. (a) Schematic illustration, (b) SEM, (c) TEM, and (d) HRTEM images of the Si@MXene composite. (e) Schematic illustration and (f–h) TEM images of Si@MXene capsule. (Reprinted with permission from Ref. [64], Copyright 2020 ACS Publishers. Reprinted with permission from Ref. [65], Copyright 2020 ACS Publishers).

Coating silicon with MXene nanosheets has been proven to be a useful strategy by different researchers [66,67]. Both the core-shell and capsule structures could provide satisfactory interface modification for the formation of more stable SEI layers.

The advantages and disadvantages of the four structures of Si/MXene composites are summarized in Table 1. Among the above four structures, the coating structure is easy to achieve for combination with other materials to form composites but the stability and integrity of the whole active material are difficult to control. The self-standing film has great superiority with no need for a binder and current collector but is difficult to align with the current manufacturing process of LIBs. The layer-by-layer and 3D structures make great use of the merits of MXene, and we believe a 3D structure is better suited to high performance Si/MXene composites due to the flexibility and compatibility with other materials.

Table 1. Summary of advantages and disadvantages of different structures of Si/MXene composites.

Structure	Advantages	Disadvantages
Layer-by-Layer	<ul style="list-style-type: none"> • The loose layered structure can account for the volume expansion of SiNPs and prevent aggregation; • The electronic transport pathway can effectively promote carrier transfer; • Layered structure can help maintain the stability and integrity of the whole composite structure; • Large specific surface area. 	<ul style="list-style-type: none"> • Volumetric capacity should be considered.
Self-standing	<ul style="list-style-type: none"> • Highly conductive MXene can act as a matrix and the current collector, overcoming the effect of inactive binders. 	<ul style="list-style-type: none"> • Preparation of the large-area uniform film could be difficult; • Consideration of matching with existing processes should be considered.
3D	<ul style="list-style-type: none"> • MXene nanosheets interconnect into a skeleton-like frame, with SiNPs inside the skeleton by bonding and adherent to MXene plate; • The porous structure provides conductive pathways and a larger specific surface area for more active reaction sites. 	<ul style="list-style-type: none"> • The connection and synergistic effect between the components should be considered.
Coating	<ul style="list-style-type: none"> • MXene can work as a robust and flexible layer to accommodate the volume expansion of silicon to prevent pulverization; • MXene layer can effectively prevent nanoparticles from directly contacting the electrolyte and thus enable the formation of a stable SEI film. 	<ul style="list-style-type: none"> • The possible aggregation and the interconnection of capsule structures should be considered.

2.2. Preparation Methods

To obtain differently structured composites, various preparation theories and methods have been utilized, including mechanical mixing [47,60], vacuum-assisted filtration [54], the preparation of SiO_x/MXene by hydrolysis followed by magnesiothermic reduction [48,61], solution treatment, freeze-drying [46,58], spray-drying [65], wet-processing [41,50], and electrospinning [62]. More specifically, free-standing Si/MXene composite films are usually fabricated by the filtration of the suspension of Si and MXene. Freeze-drying can lead to a porous 3D structure, and magnesiothermic reduction always maintains the microstructure and morphology of the precursor MXene/SiO_x composites. A further discussion on Si/MXene preparation is provided below.

2.2.1. Mechanical Mixing

Mechanical mixing is one of the most facile, scalable, and widespread methods for the preparation of various silicon-based composites. Silicon and MXene in powder forms can

be mechanically composited by simple mixing, ball-milling, or grinding. Energy derived from the mechanical impact could transfer to silicon and MXene, helping the components to connect. In particular, high-energy ball milling can both reduce the reaction activation energy and increase the adhesion of Si to MXene, forming the continuous electric network.

In 2018, Kong et al. first reported on the combination of Si and Ti_3C_2 MXene as a negative material in LIBs [47]. As shown in Figure 7a, by mixing Si powders and accordion-like MXene nanosheets in alcohol, composites with a layer-by-layer structure were obtained after vigorous stirring and ultrasonication. In 2019, Liu et al. prepared MXene/Si/CNTs composites with planetary ball-mill using partially etched accordion-like MXene nanosheets, SiNPs, and CNTs as starting materials. During ball-milling, tungsten carbide balls provided appropriate energy to reinforce the combination of the three components into a chemical-bond-restricted composite with a 3D porous structure [60]. Figure 7b illustrates how the mechanochemical process via ball milling of Si, MXene, and CNT produces 3D porous composites. In such a porous composite, Si particles are reactive enough to instantly select Ti atoms from MXene to form Ti–Si bonds and C atoms from CNT to form C–Si bonds.

Generally, mechanical mixing is very attractive due to its simplicity, low energy consumption, affordable cost, environmental friendliness, and the potential for mass production. However, despite these advantages, several challenges should be considered, including the introduction of extra impurities and the poor diversity in the resulting structure.

2.2.2. Wet Processing Method

The wet processing method is another facile, easy-to-operate procedure for the synthesis of silicon-based composites. By dispersing the powders of silicon, MXenes, and other components in the same solvent, a uniform solution/slurry can be formed, which leads to efficient mixing and self-assembly. After solvent evaporation, centrifugation, or filtration, the composite powder can be obtained for further treatment.

In 2020, Cui et al. carried out a self-assembly process in solution and received a Si/MXene composite with a layer-by-layer structure [41]. SiNPs were firstly treated with 3-aminopropyltriethoxysilane (APTES), and a methanol solution containing NH_2 -SiNPs was added dropwise into the dispersion of thin MXene nanosheets. As shown in Figure 7c, the positively charged NH_2 -Si can then be uniformly anchored on the surfaces of negatively charged $\text{Ti}_3\text{C}_2\text{T}_x$ nanosheets. After repeating this attraction and deposition process, a layer-by-layer structured Si/MXene composite can electrostatically self-assemble.

Similar attempts were made by several groups, which all proved the wet processing method to be effective and reproducible. Zhang et al. [45] used accordion-like MXene nanosheets derived from etching Ti_3AlC_2 and amine functionalized SiNPs by dropwise hybridization to prepare the composite. The SiNPs were decorated on $\text{Ti}_3\text{C}_2\text{T}_x$ nanosheets by electrostatic bonding. Recently, Jo et al. prepared a ternary composite of Si@N-doped C with 2D MXene nanosheets through wet processing [57]. Si@PDA (polydopamine) nanoparticles were first synthesized and then slowly added into a suspension of MXene nanosheets under stirring for 1 h. Strong chemical bonding formed to connect the Si@PDA particles and MXene nanosheets. The composites were then heated to carbonize the PDA layer, resulting in a 3D structure with the MXene framework and carbon coating.

As a remarkably simplified and contamination-free procedure, the wet processing method is suitable for commercial production. Meanwhile, the terminal surface groups of MXene make it easy to assemble with silicon into desired structures. The process should be controlled precisely to ensure the uniformity and desired structure of the synthesized products. Methods that require a lower energy input for a more efficient recovery of the solvent are also needed to mitigate any possible environmental impact.

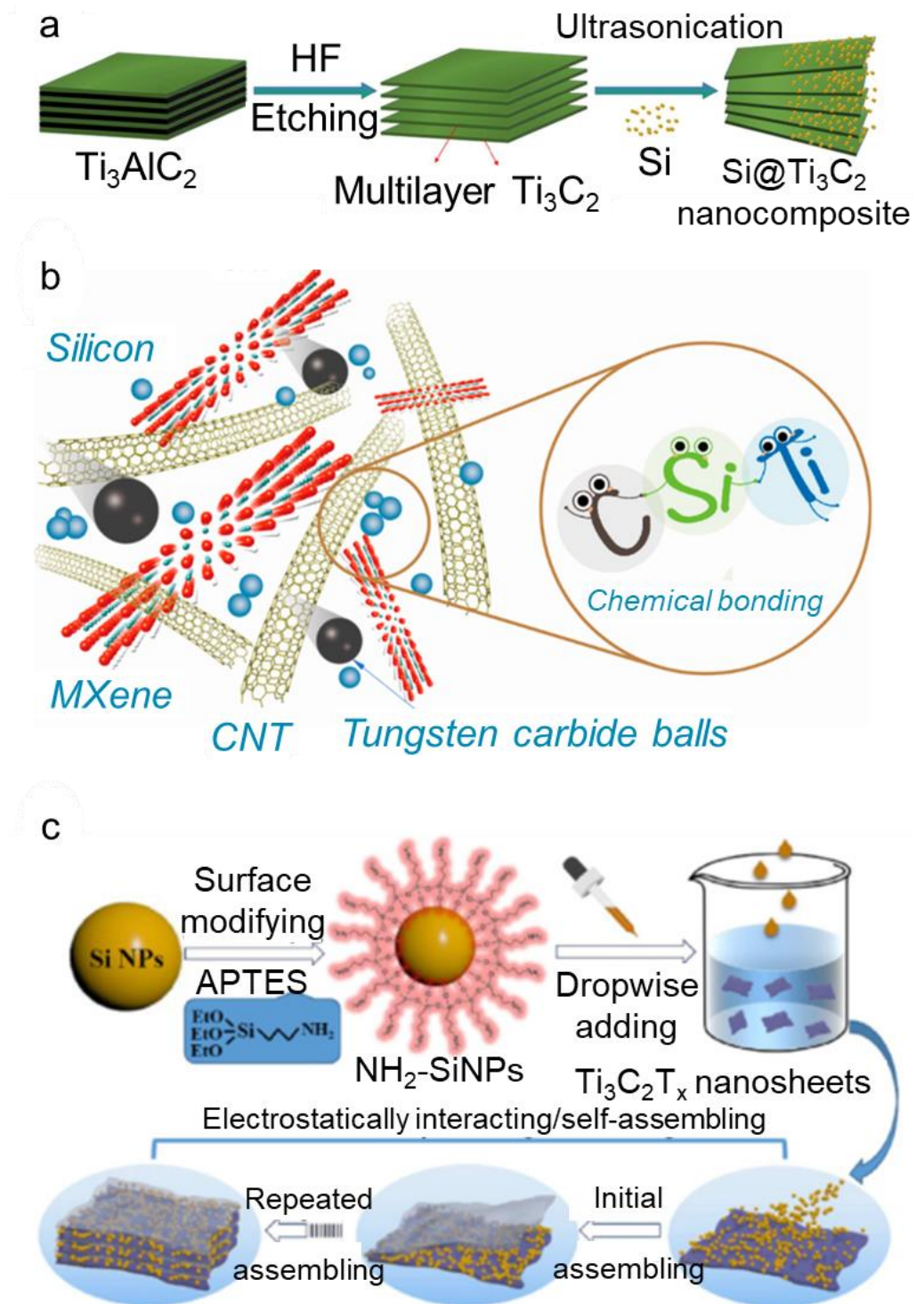


Figure 7. Preparation of Si/MXene composites. (a) Preparation scheme for Si@Ti₃C₂ nanocomposite. (b) Schematic mechanochemical composite formation by ball-milling of MXene in the presence of Si and CNT. (Reprinted with permission from Ref. [47], Copyright 2018 Elsevier; reprinted with permission from Ref. [60], Copyright 2019 ACS Publishers, respectively.) (c) Illustration of synthesis of self-assembled NH₂-Si/Ti₃C₂T_x. (Reprinted with permission from Ref. [41], Copyright 2020 John Wiley and Sons).

2.2.3. Spray Drying Method

Spray drying is another frequently used and scalable preparation technique for Si/MXene powders [68]. Similar to the wet processing method, the starting materials

are firstly mixed in solution for self-assembly or chemical interconnection. The composite materials can be dried and dispersed into dry, fine powders by quickly removing the solvent from the solution. The resulting dry particles are often uniform in size and morphology (usually spherical) and only require a one-step process.

Yan et al. fabricated Si@MXene with a coating structure by spray drying [65]. The single- or few-layer MXene nanosheets solution was obtained by etching the MAX phase, and SiNPs were dispersed in deionized water and then dropwise added into the MXene solution. After stirring for 8 h, the mixture suspension was spray-dried at 220 °C, leading to composites with a capsule structure.

Recently, they performed the following heat treatment on these capsule-structured composites [67]. After annealing at 1000 °C for 3 h under an Ar/5% H₂ atmosphere, the Si@MXene composite transformed into an Si@TiO₂-TiSi₂ composite, which also exhibited high capacity retention after long cycling at large specific currents.

The spray drying method provides an environmentally friendly, high yield, easy, and continuous way by which to prepare powders with a modified micro-morphology and porous structure, showing a great prospect in large-scale production. However, in the reaction chamber, a large amount of hot air has no effect on drying of the powders, so the thermal efficiency is not high enough. Besides, it is difficult to construct 1D or 2D structures of Si/MXenes, which may better utilize the advantages of MXene.

2.2.4. Magnesiothermic Reduction Method

Magnesiothermic reduction is widely investigated as a promising process for making porous silicon with micro- or nanosized structures that promote the further formation of various silicon-based composites [69]. In a reducing ambient at relatively mild temperatures (600 to 700 °C), silica with various sizes, morphologies and crystalline structures are reduced by the magnesium (Mg) vapour via the following reaction [70].



In the process of Si/MXene composite synthesis, TEOS (Si(OC₂H₅)₄), tetraethyl orthosilicate) is hydrolysed to produce SiO₂ which can then be coated on the MXene template in the same reaction solution. After magnesiothermic reduction, the obtained silicon retains the microstructure of the SiO₂ precursor.

As shown in Figure 8a, Zhang et al. hydrolysed TEOS on accordion-like MXene nanosheets and then conducted an in situ magnesiothermic reduction procedure to convert SiO_x/MXene to Si/MXene [48]. In the process, they observed that SiO_x hydrolysed from TEOS deposited on each open lamellar Ti₃C₂T_x nanosheet and was reduced in situ to SiNPs which were uniformly anchored on the surface of the MXene nanosheet.

Hui et al. synthesized a novel hierarchical porous Ti₃C₂/Si composite by a similar process [56]. After the etching and intercalation process, thin Ti₃C₂ nanosheets were obtained. By adding TEOS in the MXene suspension solution, the controlled hydrolysis process resulted in the heterogeneous nucleation and growth of SiO₂ on the surfaces of individual MXene plates. Then, a low-temperature magnesiothermic reduction reaction (at about 200 °C) reduced silica into monodispersed SiNPs (d ≈ 40 nm) which were anchored on Ti₃C₂ nanosheets via Si-O-Ti bonds. In 2020, Jiang et al. [61] prepared a Ti₃C₂@Si/SiO_x composite in the same hydrolysis and uncompleted magnesiothermic reduction process and then added TiO₂ coating on the laminar composite to form a novel Ti₃C₂@Si/SiO_x@TiO₂ composite.

The magnesiothermic reduction method is a low-cost, simple, and convenient process, which can produce controllable morphology according to the precursor. However, obstacles exist for the magnesiothermic reduction process in terms of realizing large-scale production due to the low silicon yield, by-products, and the difficulty in precisely controlling the reaction.

2.2.5. Filtration Method

The filtration method is an effective and facile way by which to directly prepare free-standing film instead of powders [55]. Based on the wet processing method, silicon and MXene self-assemble in the mixing solution and form a thin free-standing film during the vacuum filtration procedure. According to Figure 8b, by etching MAX, stirring, centrifugation, and hand-shaking, researchers obtained the MXene colloidal solution which was mainly composed of single- or few-layer $Ti_3C_2T_x$ flakes [54]. After adding SiNPs to the colloidal solution and stirring, a flexible and freestanding paper can be prepared by vacuum filtration using a PVDF membrane. In the Si/MXene paper, Si nanospheres were dispersed randomly between parallel MXene sheets, and the mass loading of the active Si/MXene composite material was approximately 1.1 to $1.3 \text{ mg}\cdot\text{cm}^{-2}$.

Other components such as carbon can be added to the free-standing film. Cao et al. prepared the self-assembled $Ti_3C_2T_x$ -CNT/SiNPs film by vacuum filtration [55]. The flexible and conductive CNTs and MXenes could act as the buffer matrix and carrier transportation channels simultaneously, leading to better electrochemical performance. Zhang et al. used Si@C nanoparticles as precursors and carried out vacuum filtration together with the single- or few-layer MXene nanosheets solution [53]. The achieved MXene-bonded Si@C film presented the porous structure and high conductivity for a higher rate performance.

The great virtue of this vacuum-assisted filtration method is the fact that one can directly obtain an electrode film in a facile process without slurry preparation and coating. The free-standing film is always flexible and conductive, without binder and other conductive additives, leading to a larger mass ratio of active material. However, it may not be easy for commercial development, and the thickness and mass loading should be controlled precisely during solution preparation and filtration.

2.2.6. Freeze-Drying Method

Another technique based on the wet process, freeze-drying, is a drying technique by freezing the product into solid-state by which the solvent (usual water) is removed by sublimation. Freeze-drying is a common method for the preparation of composite materials with hierarchical porous structures [71].

Numerous Si/graphene composites with aerogel structures have been prepared through the freeze-drying process [72]. Considering the structural similarity of MXene with graphene, Si/MXene 3D porous composites can be obtained by the same method.

As shown in Figure 8c, Wang et al. mixed the MXene suspension which was obtained by MAX-etching and ultrasonication with SiNPs suspension and quickly freezing the mixture with liquid nitrogen [58]. After drying at 10 Pa and -50°C for 36 h, a Si@ $Ti_3C_2T_x$ composite with a 3D porous structure was prepared.

Li et al. prepared 3D dual MXene/Si composites for LIBs negatodes [59]. Firstly, they prepared SiNP@MXene1 by electrostatic self-assembly. Then, by mixing SiNP@MXene1 with MXene in a colloidal solution, they performed a hydrothermal reaction and freeze-drying to achieve the 3D hierarchically porous structure (SiNP@MXene1/MXene2).

The freeze-drying method is facile, environmentally friendly, controllable, and easy to use for the construction of porous frame structures which can accommodate the large volume change of silicon-based negatodes with a high specific surface area. Nevertheless, freeze-drying often requires more time, and the yield is not high enough. For mass production, the constitution and the interaction between the components in the precursor solution should be designed carefully.

In the above methods, spray drying and magnesiothermic reduction are easily adopted for the construction of special microstructures, while mechanical mixing and wet processing are more promising for mass production. The filtration method can directly prepare the Si/MXene film without a binder. The advantages and disadvantages of different methods for preparing Si/MXene composites are summarized in Table 2. In addition, by combining the advantages of different methods, the multiple-step technique is another attractive way to synthesize Si/MXene composites. The balance of simplicity and electrochemical

performance should be considered, and therefore, we believe the wet processing method is more promising for the commercial production and application of Si/MXene composites.

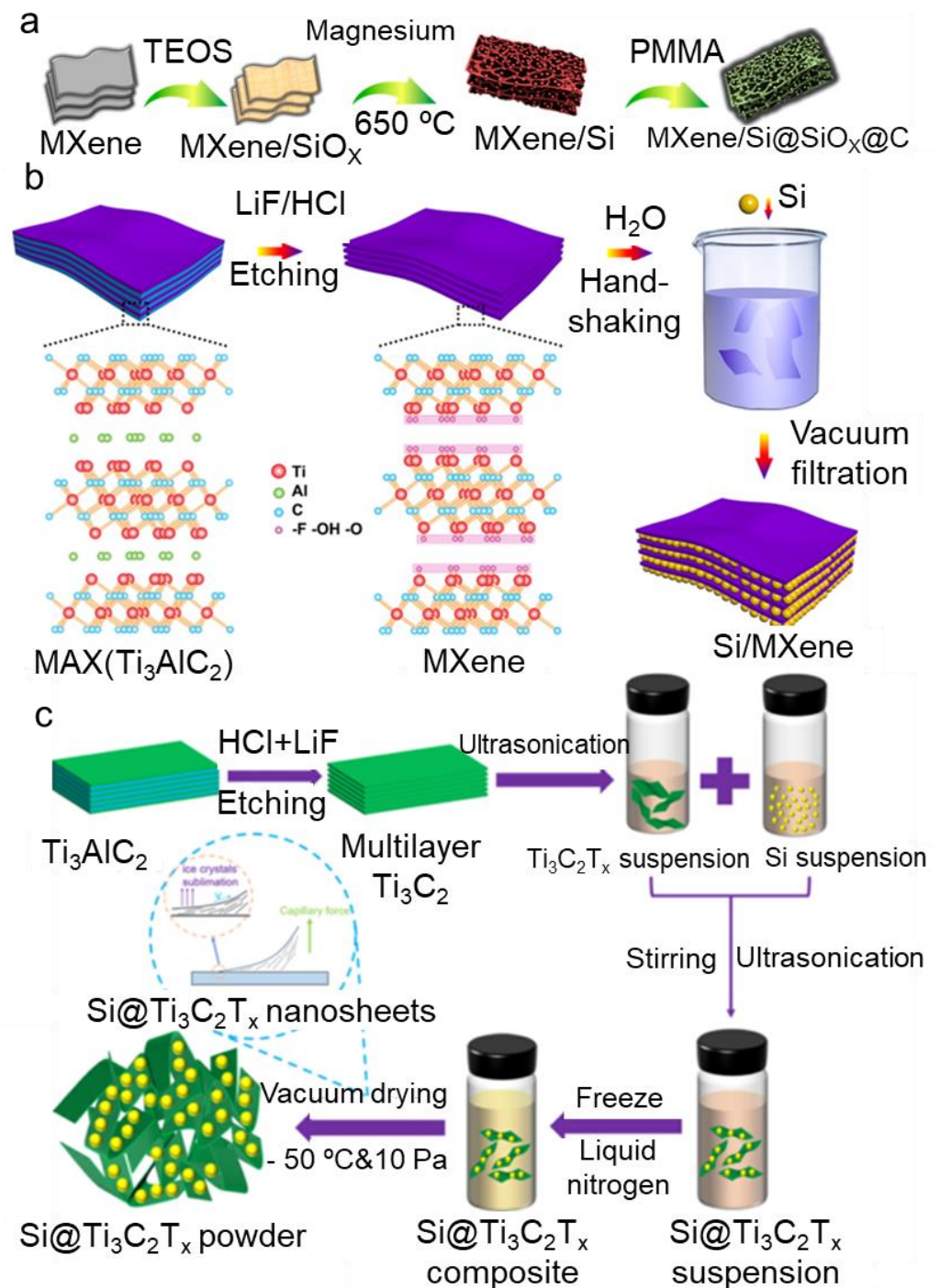


Figure 8. Preparation of Si/MXene composites. (a) Schematic preparation procedure for MXene/Si@SiO_x@C nanohybrids. (Reprinted with permission from Ref. [48], Copyright 2019 ACS Publishers). (b) Schematic preparation routes for Si/MXene composite paper and (c) Si@Ti₃C₂T_x powder. (Reprinted with permission from Ref. [54], Copyright 2019 ACS Publishers; reprinted with permission from Ref. [58], Copyright 2021 Elsevier, respectively).

2.3. Interface Modification of Si in Si/MXene Composites

In Si/MXene composites prepared via simple mixing, SiNPs are always chemically anchored by the Ti-Si bond. During lithiation, MXene could buffer the volume change of silicon to some extent and the whole composite can retain integrity without pulverization.

However, there still exists the exfoliation phenomenon of SiNPs from MXene nanosheets due to insufficient bonding. Besides, the MXene framework may restrain the volume expansion of silicon and improve electron transportation but could not prevent the repeated formation of the SEI layer on the surface of silicon. Therefore, the modification of the interface between silicon and MXene nanosheets is necessary to strengthen their mutual interactions and control the surface reaction of silicon.

Table 2. Summary of advantages and disadvantages of different preparation methods.

Preparation Methods	Advantages	Disadvantages
Mechanical mixing	Facile; Scalable; Low cost; Environmental friendliness.	Possible introduction of extra impurities; Poor diversity in the resulting structure.
Wet processing	Facile; Suitable for commercial production; Desired structures from bonding between terminal surface groups of MXene and silicon nanoparticles.	Precise control needed to ensure uniformity and desired structure; Consideration of solvent recovery and energy consumption should be considered.
Spray drying	Environmentally friendly; High yield; Easy and continuous; Modified micro-morphology and porous structure.	Low thermal efficiency; Inconvenient to construct 1D or 2D structures of Si/MXenes.
Magnesiothermic reduction	Low-cost; Simple, and convenient process, Controllable morphology.	Difficult to realize large-scale production; Low silicon yield and by-products; Precise control needed of the reaction.
Filtration	Facile and direct formation of electrode films; High loading of active material without binder and conductive additives.	Not easy for commercial development; Precise control needed of the thickness and mass loading during solution preparation and filtration.
Freeze-drying	Facile and Controllable; Environmentally friendly; Easy construction of porous frame with high specific surface area.	Long time; Unsatisfactory yield; Careful selection of precursor solution needed for mass production.

2.3.1. Si Surface Modification—Positive Charged

Many studies have been performed regarding the surface modification of silicon to decorate SiNPs with positive charges. The surface of $Ti_3C_2T_x$ MXene nanosheets can be terminated with several functional groups including -O, -OH, and -F, and they are negatively polarized. The original SiNPs process negative surface charges due to the existence of a natural oxide layer outside silicon. By modifying with a surfactant such as CTAB, phthalic diglycol diacrylate (PDDA), and APTES, positively charged SiNPs could be obtained, which can then interact more tightly with MXene nanosheets, which in turn could improve charge transfer and structural stability.

In 2018, Zhang et al. [45] treated SiNPs by boiling an H_2SO_4/H_2O_2 (3:1 in volume) solution and subsequently a toluene solution containing 1 wt.% APTES to achieve the hydroxyl and amine functionalized SiNPs, respectively. As shown in Figure 9a, while adding SiNPs dropwise into the suspension of accordion-like MXene nanosheets, the positively charged SiNPs could uniformly deposit on the surfaces of each layer of MXene nanosheets. Cui et al. also performed APTES modification to achieve positive NH_2 -Si (Figure 9b) [50], which then slowly adhered to MXene nanosheets by electrostatic self-assembly to form NH_2 -Si/ $Ti_3C_2T_x$ composites. According to the FTIR spectrum, there was

an obvious peak shift of the Ti-O and Si-O bonds after the electrostatic assembly of NH₂-Si and Ti₃C₂T_x. They also mentioned that this electrostatic self-assembly process required more time to achieve complete attraction between the two species, which is different from the layer-by-layer assembly.

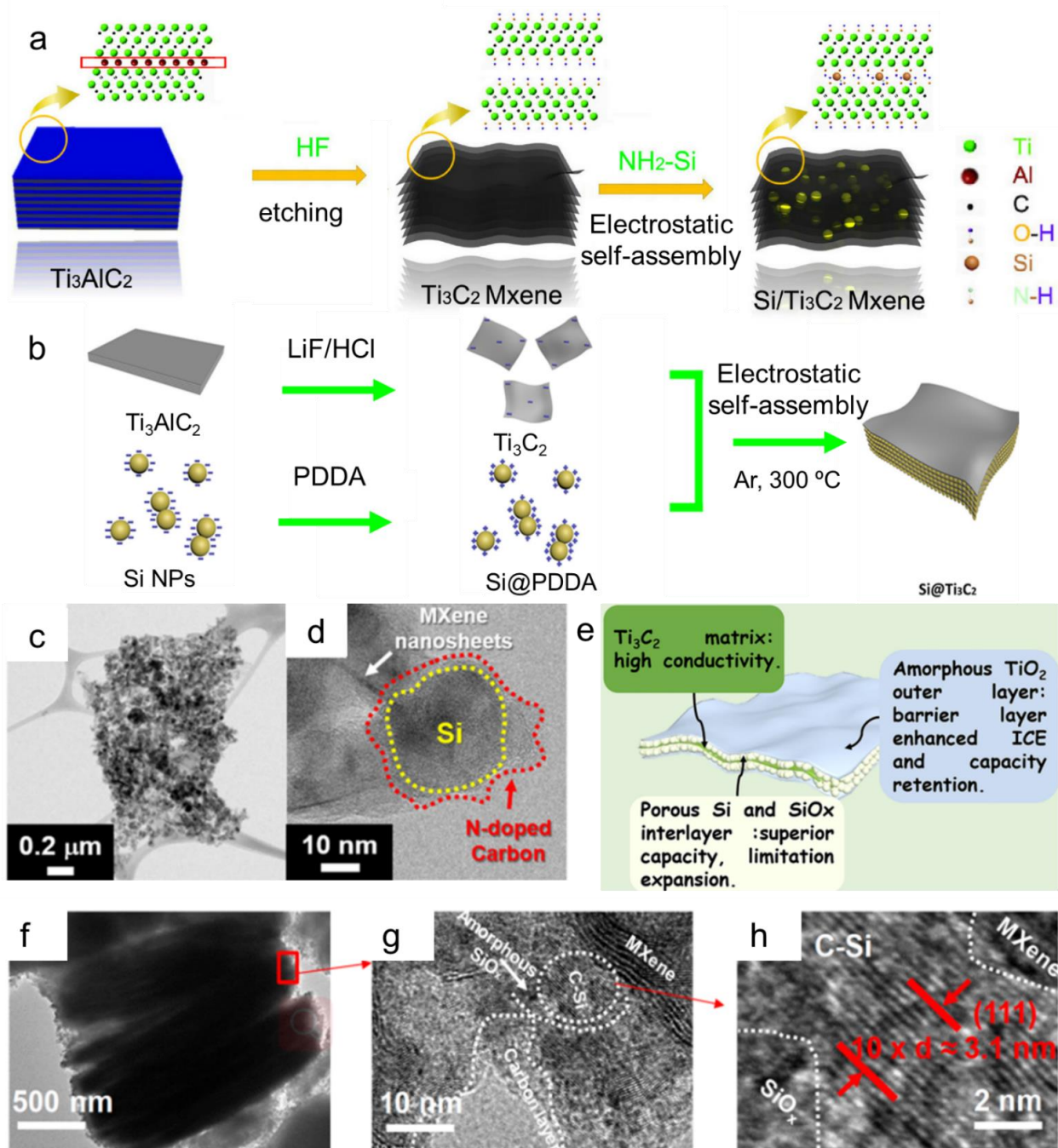


Figure 9. Surface modification of silicon. Schematic illustrations of (a) synthesis of the Si/Ti₃C₂T_x composite, and (b) fabrication of Si@Ti₃C₂ superstructures. (Reprinted with permission from Ref. [45], Copyright 2020 Elsevier. Reprinted with permission from Ref. [50], Copyright 2020 Elsevier, respectively). (c) TEM and (d) HRTEM images of Si@NC/MXene. (Reprinted with permission from Ref. [57], Copyright 2021 Elsevier). (e) Schematic explanation of the structural functions in the Ti₃C₂@Si/SiO_x@TiO₂ composite. (f) TEM and (g,h) HRTEM images of MXene/Si@SiO_x@C-2. (Reprinted with permission from Ref. [61], Copyright 2020 ACS Publishers, reprinted with permission from Ref. [48], Copyright 2019 ACS Publishers, respectively).

Li et al. [59] used CTAB, a cationic surfactant, to modify SiNPs (CTAB-SiNP) with positive charges. The surface terminal groups with negative charges on the single- or few-layer MXene nanosheets can capture the positively charged SiNPs with strong coulombic attraction, resulting in a wrapping structure of Si@MXene. Cao et al. prepared $\text{Ti}_3\text{C}_2\text{T}_x\text{-CNT/SiNPs}$ composites [55]. The modified CNTs were attached with a large number of carboxyl groups, which helped form hydrogen bonds with MXene nanosheets. Then, the surface charges on SiNPs were adjusted from negative to positive by stirring in the CTAB solution. Due to the electrostatic interactions between positively charged SiNPs and negatively charged MXene/CNTs nanosheets, SiNPs tightly and homogeneously adhered on the surface of MXene nanosheets.

In addition, 3-aminopropyltrimethoxysilane (APS) and PDDA can provide surface modifications of silicon by a similar mechanism [66]. For example, in Figure 9c, the few-layer MXene nanosheets with negative charges electrostatically interact with positively charged Si@PDDA nanoparticles, leading to a self-assembly process [57].

Achieving tighter interactions between Si and MXene via electrostatic attraction is a facile, controllable, low-cost, and effective strategy for surface modification of silicon. Generally, the surfactant can be removed or carbonized during following treatments such as annealing.

2.3.2. Coating on the Surface of the Silicon

Another strategy for Si/MXene interface engineering is to deposit a coating layer on the surface of silicon. The single- or few-layer MXene nanosheets and other materials such as carbon and SiO_x could wrap around SiNPs to form a fully enclosed structure. The coating can limit the volume change of silicon during lithiation and delithiation and prevent the direct contact of silicon with the electrolyte and help to form a more stable SEI layer. The MXene nanosheets working as coating layers have been discussed in Section 2.1.4, and in this section, other coating materials and their effects are introduced.

Zhang et al. prepared Si@C nanoparticles by self-polymerization and the carbonization of dopamine and then constructed a 3D conductive framework with few-layer MXene nanosheets with Si@C embedded inside by vacuum filtration [53]. The carbon coatings on SiNPs accounted for 24.8 wt.% of the total mass of Si@C nanocomposites according to a thermogravimetric analysis. The carbon coating could improve the bonding between Si and MXene, and prevent the fracture of silicon during the cycling. By mixing SiNPs with a dopamine hydrochloride solution, Jo et al. firstly obtained Si@PDA [57]. Upon mixing the suspensions of MXene and Si@PDA, the Si@PDA/MXene composite immediately precipitated due to the strong chemical bonding between PDA and MXene. Annealing the precipitate under an Ar atmosphere at 600 °C for 2 h transformed the PDA layer to N-doped carbon and finally the Si@NC/MXene composites were obtained. From the TEM images of this Si@NC/MXene composite in Figure 9c,d, it can be observed that individual SiNPs were coated by an amorphous N-doped carbon layer, all located on MXene thin nanosheets. It demonstrated that SiNPs and few-layer MXene nanosheets interacted intimately via chemical bonding, leading to anchored SiNPs on MXene without aggregation. The dual protection from N-doped carbon layer and MXene nanosheets can alleviate the high level of volume expansion of silicon and enhance the carrier transportation.

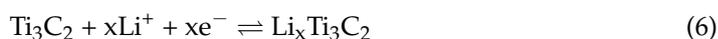
After magnesiothermic reduction, Jiang et al. conducted the sol-gel process with tetrabutyl titanate (TBT) as the titanium precursor on the surface of silicon in $\text{Ti}_3\text{C}_2\text{@Si/SiO}_x$ composites [61]. The resulting $\text{Ti}_3\text{C}_2\text{@Si/SiO}_x\text{@TiO}_2$ composites presented a sandwiched structure as shown in Figure 9e, in which $\text{Ti}_3\text{C}_2\text{T}_x$ nanosheets constructed the conductive network as the matrix. The porous Si and SiO_x could provide high capacity, while the amorphous TiO_2 outer layer could act as a barrier layer to provide a more stable SEI layer and enhance the initial coulombic efficiency (ICE) as well as capacity retention. Zhang et al. [48] formed SiO_x coating via the direct pyrolysis of the poly(methyl methacrylate) (PMMA) polymer on the surface of Si/MXene composites using urea as nitrogen source. During the pyrolysis process, the ester group in PMMA can be thermally decomposed to carbon

with the simultaneous formation of SiO_x , resulting in the MXene/Si@ SiO_x @C composites. From the TEM and HRTEM images shown in Figure 9f–h, thin SiO_x and carbon layers encapsulated Si/MXene, forming a micro 3D porous sandwich-like structure in the whole laminar composites. The lattice plane of SiNPs could be clearly observed and attributed to Si (111), indicating good crystallinity of silicon. Both the SiO_x layer and carbon layer exhibited amorphous structures, which could tolerate the strain from the silicon lithiation process to a larger extent.

3. Electrochemical Performance of Si/MXene Composites as Negatropes in LIBs

The electrochemical behavior and performance of typical Si/MXene composite negatropes for LIBs are summarized in Table 3. In 2014, Sun et al. [73] demonstrated the Li storage behavior of 2D Ti_3C_2 obtained by etching and intercalating with dimethyl sulfoxide via cyclic voltammetry (CV) and galvanostatic charging and discharging (GCD) cycling. Figure 10a shows the CVs of the first three cycles from 3.0 V to 0.01 V vs. Li/Li^+ at a scan rate of 0.2 mV s^{-1} . In the first cycle, there were broad cathodic peaks at 1.66 V and 0.62 V, which almost disappeared in the following cycles, suggesting SEI formation during the initial intercalation process of Li^+ ion into the MXene nanosheets. The anodic peaks at 1.96 V and 2.44 V were attributed to the extraction of Li^+ ion from Ti_3C_2 nanosheets which became slightly decreased in the second and third cycles. Besides, the reduction peak at 0.01 V was assigned to the lithiation of carbon (Super P), which would require the presence of the graphitic structure in the carbon. The initial charge and discharge capacities were 264 and 124 mAh g^{-1} of in- Ti_3C_2 (intercalated with DMSO after exfoliation), with an ICE of 47%. After 75 cycles, it only delivered 89.7 mAh g^{-1} . The in- Ti_3C_2 nanosheets exhibited similar capacities in the first cycle but higher capacity retention after 75 cycles with a discharge capacity of 118.7 mAh g^{-1} . The low ICE is a result of the formation of the SEI film and the irreversible reduction of electrochemically active surface groups. Besides, surface functional groups and treating process of MXene nanosheets also influence their electrochemical behavior [74].

After compositing with silicon, due to the more obvious electrochemical reaction process and higher capacity of silicon, the lithiation and delithiation peaks of MXene are likely to be neglected. However, the SEI layer formed on surface Ti_3C_2 nanosheets is more stable and beneficial for Li^+ ion transportation in the composites. Kong et al. [47] investigated the directly composited Si@MXene by CV and GCD, as shown in Figure 10c,d. The electrochemical reaction of Si@MXene during lithiation and delithiation is listed as the following equations [59].



Si and Ti_3C_2 would transform to Li_xSi and $\text{Li}_x\text{Ti}_3\text{C}_2$ during lithiation and back to initial Si and Ti_3C_2 after Li extraction. In Figure 10c, there is a broad cathodic peak visible at 1.45 V in the first cycle which could be assigned to the irreversible reaction of the active surface functional groups of MXene nanosheets with electrolyte [47]. The adjacent reduction peak at around 1.10 V and 0.84 V is attributed to the formation of the SEI layer via reaction between Ti_3C_2 , Si, and electrolyte, respectively [47]. Except for these three cycles, which disappear in the subsequent cycles, the cathodic peaks at 0.17 V correspond to the lithiation of Si to Li_xSi , while the two peaks at 0.37 V and 0.54 V in anodic sweep could be assigned to the delithiation of Li_xSi back to amorphous Si in the composites [47]. The broad anodic peak around 0.98 V was associated with Li^+ ion extraction between the Ti_3C_2 layers. Figure 10d shows the first three GCD curves of Si@MXene at a specific current of 200 mA g^{-1} . In the first cycle, the charge and discharge capacities are 879 and 1195 mAh g^{-1} , respectively. The ICE of the layer-by-layer Si/MXene composites is 69%, and the columbic efficiency and reversible capacities become stable from the second cycle.

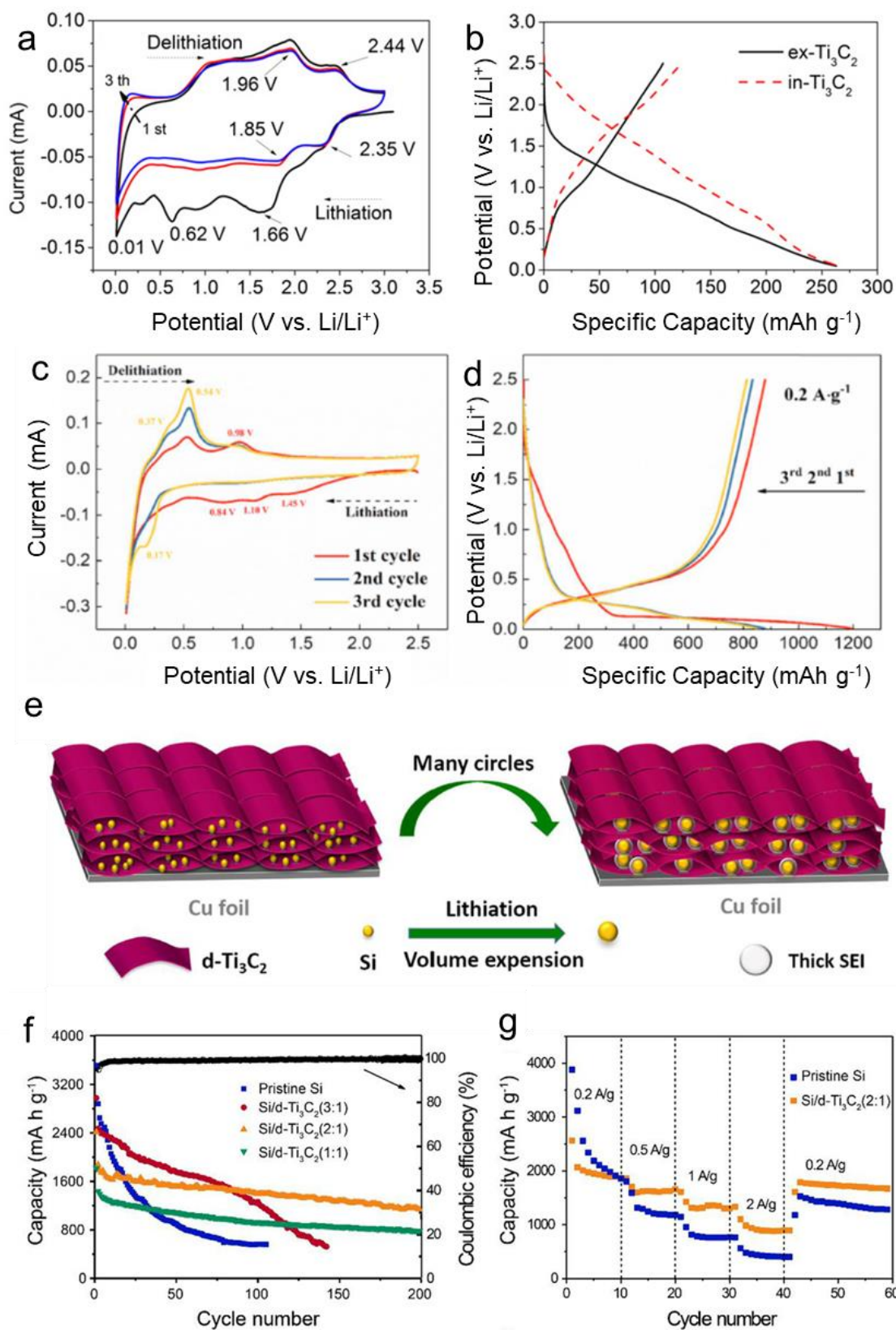


Figure 10. (a) CVs at a scan rate of 0.2 mV s^{-1} and (b) GCDs at 1 C of two types of Ti_3C_2 . (c) CVs at 0.1 mV s^{-1} and (d) GCDs at 0.2 A g^{-1} of Si@ Ti_3C_2 nanocomposite. (e) Illustration of the sandwich-like Si/ Ti_3C_2 hybrids as the electrode of LIBs. (f) Cycling performance of the Si/ Ti_3C_2 hybrids with different mass ratios at 500 mA g^{-1} . (g) Rate capability of Si/ Ti_3C_2 (2:1) hybrids and pristine SiNPs.

(Reprinted with permission from Ref. [73], Copyright 2014 Elsevier; reprinted with permission from Ref. [47], Copyright 2018 Elsevier; reprinted with permission from Ref. [46], Copyrights 2019 Elsevier, respectively).

It is interesting to note that, except for the first cathodic scan, the current peaks, either cathodic or anodic, in Figure 10c are at more negative potentials than those in Figure 10a. These differences indicate that Si undergoes lithiation and delithiation at more negative potentials than Ti_3C_2 alone. However, the first cycle CV in Figure 10c also shows three cathodic peaks at potentials comparable to those in Figure 10a. These cathodic peaks disappeared on the CVs of the second and later cycles. A plausible explanation is that the more conducting and more active Ti_3C_2 phase might have played a role of activating the inert and poorly conducting Si phase in the Si/MXene composite. Obviously, more studies are needed to confirm this hypothesis.

In another layer-by-layer structure, Zhu et al. [46] investigated the electrochemical behavior of the Si/ Ti_3C_2 composites as shown in Figure 10e. The volume expansion of SiNPs during lithiation could be restricted due to the anchoring effect to MXene nanosheets, leading to the integrated composite structure without fracture. They investigated the electrochemical properties of Si/ Ti_3C_2 with different weight ratios and compared them with pristine silicon. After 200 charge/discharge cycles at 500 mAh g^{-1} , the Si/delaminated- Ti_3C_2 (Si/d- Ti_3C_2) composite (2:1) expressed the highest reversible discharge capacity of $1137.6 \text{ mAh g}^{-1}$ (Figure 10f), which is much higher than those of pristine silicon and pure d- Ti_3C_2 . Furthermore, the Si/ Ti_3C_2 (2:1) composite also revealed higher rate capacities of 1948, 1620, 1310, 890 mAh g^{-1} at specific densities of 200, 500, 1000, and 2000 mA g^{-1} after constructing the layered composite with moderate weight ratio.

Except for the layer-by-layer structure benefiting from the original 2D structure of MXene, other structures such as the coating structure could affect the electrochemical performance of Si/MXene composites in more ways. Figure 11a shows schematically the mechanism of the lithiation process in both the nano spherical silicon and capsule-like Si@MXene composite [65]. The excellent mechanical stability of MXene nanosheets derived from the abundant covalent bonds (Ti-O-Ti) could help maintain the structure of Si/MXene negatode. More importantly, the MXene coating prevented the contact between silicon to the electrolyte, leading to a different SEI layer from that on bare silicon. MXene nanosheets are full of fluorine terminations, resulting in the stable LiF-rich SEI layer on the MXene surface due to the following reaction [75].



The stable SEI layer could hinder the repeated reaction between silicon and electrolyte and improve the reversible cycling capacity. The Si@MXene composites revealed a reversible discharge capacity of $1155.4 \text{ mAh g}^{-1}$ after 50 cycles at 0.5 A g^{-1} , of much higher than that of bare silicon, which was only 74 mAh g^{-1} due to the fracture and extra Li^+ ion consumption due to the repeated formation of the SEI layer (Figure 11b,c). After 150 cycles, the capacity of Si@MXene negatodes remained at 1004 mAh g^{-1} , with a retention rate of 81%, indicating the positive effect of stable SEI film on the MXene coating layer. Benefiting from the high electroconductivity of MXene nanosheets, Si@MXene composites also exhibited better rate performance than bare silicon, with a reversible capacity of 1791, 1412, 1053, and 759 mAh g^{-1} at the specific current of 0.2, 0.5, 1, and 2 A g^{-1} . Taking advantage of both silicon and MXene, this well-designed capsule structure could provide excellent electrochemical performance with a stable structure.

Table 3. Summary of the electrochemical performance of typical Si/MXene composite negatodes for LIBs.

Materials	Preparation Methods	Structure	Cycle Stability	Rate Capability	ICE	Ref.
Si@Ti ₃ C ₂ MXene	Mechanical mixing	Layer-by-Layer	0.2 A g ⁻¹ , 150 cycles, 188 mAh g ⁻¹	3 A g ⁻¹ , ~100 mAh g ⁻¹	69%	[47]
MXene bonded Si@C film	Filtration	Free-standing film	420 mA g ⁻¹ , 150 cycles, 1041 mAh g ⁻¹	8.4 A g ⁻¹ , ~500 mAh g ⁻¹	73%	[53]
MXene-Si-CNT	Mechanical mixing	3D Porous	2 A g ⁻¹ , 200 cycles, 841 mAh g ⁻¹	2 A g ⁻¹ , ~800 mAh g ⁻¹	70.38%	[60]
MXene&Si	Filtration	Free-standing film	100 mA g ⁻¹ , 500 cycles, 558 mAh g ⁻¹	5 C, ~150 mAh g ⁻¹	61%	[52]
Si/d-Ti ₃ C ₂	Freeze-drying	Layer-by-Layer	500 mA g ⁻¹ , 200 cycles, 1130 mAh g ⁻¹	2 A g ⁻¹ , 890 mAh g ⁻¹	74.10%	[46]
Si/MXene	Filtration	Free-standing film	1 A g ⁻¹ , 200 cycles, 1672 mAh g ⁻¹	5 A g ⁻¹ , 886 mAh g ⁻¹	71%	[54]
nSi/MX-C	Mechanical mixing	Layer-by-Layer	1.5 A g ⁻¹ , 70 cycles, 1106 mAh g ⁻¹	3 A g ⁻¹ , 1300 mAh g ⁻¹	81–83%	[49]
Ti ₃ C ₂ /Si	Magnesiothermic reduction	3D porous	1 A g ⁻¹ , 800 cycles, 956 mAh g ⁻¹	2 A g ⁻¹ , ~450 mAh g ⁻¹	61.10%	[56]
SiO ₂ /MXene	Spray drying	Coating	1 A g ⁻¹ , 200 cycles, 635 mAh g ⁻¹	3 A g ⁻¹ , ~500 mAh g ⁻¹	71%	[68]
MXene/Si@SiO _x @C	Magnesiothermic reduction	Layer-by-Layer	10 C, 1000 cycles, 390 mAh g ⁻¹	10 C, ~400 mAh g ⁻¹	81.30%	[48]
NH ₂ -Si/Ti ₃ C ₂ T _x	Wet processing	Layer-by-Layer	0.1 C, 100 cycles, 864 mAh g ⁻¹	5 C, ~100 mAh g ⁻¹	75.20%	[41]
Si@Ti ₃ C ₂	Wet processing	Layer-by-Layer	1 A g ⁻¹ , 200 cycles, 1343 mAh g ⁻¹	3 A g ⁻¹ , ~1500 mAh g ⁻¹	73.40%	[50]
Ti ₃ C ₂ @Si/SiO _x @TiO ₂	Magnesiothermic reduction	Sandwiched	0.1 A g ⁻¹ , 100 cycles, 939 mAh g ⁻¹		66.30%	[61]
Ti ₃ C ₂ T _x /10%Si scrolls	Freeze-drying	Scroll	400 mA g ⁻¹ , 600 cycles, ~200 mAh g ⁻¹	5 A g ⁻¹ , ~80 mAh g ⁻¹		[63]
NH ₂ -Si/Ti ₃ C ₂ T _x	Wet processing	Layer-by-Layer	0.3 A g ⁻¹ , 100 cycles, 644 mAh g ⁻¹		72.70%	[45]
SiO/wrinkled MXene	Wet processing	3D Porous	0.3 A g ⁻¹ , 100 cycles, ~850 mAh g ⁻¹	2 A g ⁻¹ , ~1000 mAh g ⁻¹	69.40%	[76]
Ti ₃ C ₂ T _x -CNT/SiNPs	Filtration	Free-standing film	0.1 A g ⁻¹ , 150 cycles, 2.18 mAh cm ⁻²	2 A g ⁻¹ , ~1 mAh cm ⁻²	62.80%	[55]
SiNP@MX1/MX2	Freeze-drying	3D Porous	0.5 A g ⁻¹ , 200 cycles, 1422 mAh g ⁻¹	5 A g ⁻¹ , ~500 mAh g ⁻¹	67.20%	[59]
Si p-NS@TNSs	Mechanical mixing	Coating	0.2 A g ⁻¹ , 150 cycles, 1154 mAh g ⁻¹		80.20%	[64]
MXene/L-Si/C	Filtration	Layer-by-Layer	500 mA g ⁻¹ , 500 cycles, ~100 mAh g ⁻¹		~82%	[51]
Si@NC/MX	Wet processing	3D Porous	1 A g ⁻¹ , 300 cycles, 953 mAh g ⁻¹	10 A g ⁻¹ , ~900 mAh g ⁻¹	75%	[57]
Si/MXene@CNFs	Electrospinning	Fiber	1 A g ⁻¹ , 200 cycles, 440 mAh g ⁻¹	5 A g ⁻¹ , ~500 mAh g ⁻¹		[62]
Si@MXene	Freeze-drying	Coating	0.2 A g ⁻¹ , 100 cycles, 981 mAh g ⁻¹	2 A g ⁻¹ , ~1000 mAh g ⁻¹	71.30%	[66]
Si@TiO ₂ -TiSi ₂	Spray drying	Coating (Core-shell)	2 A g ⁻¹ , 100 cycles, 1004 mAh g ⁻¹		~91%	[67]
Si@Ti ₃ C ₂ T _x	Freeze-drying	3D Porous	1 A g ⁻¹ , 500 cycles, 1729 mAh g ⁻¹	2 A g ⁻¹ , ~500 mAh g ⁻¹		[58]
Si@MXene	Spray drying	Coating	2 A g ⁻¹ , 500 cycles, 400 mAh g ⁻¹			[65]
Si-N-MXene	Mechanical mixing	3D Porous	3.2 A g ⁻¹ , 900 cycles, 400 mAh g ⁻¹	6.4 A g ⁻¹ , 1469 mAh g ⁻¹	~85%	[37]

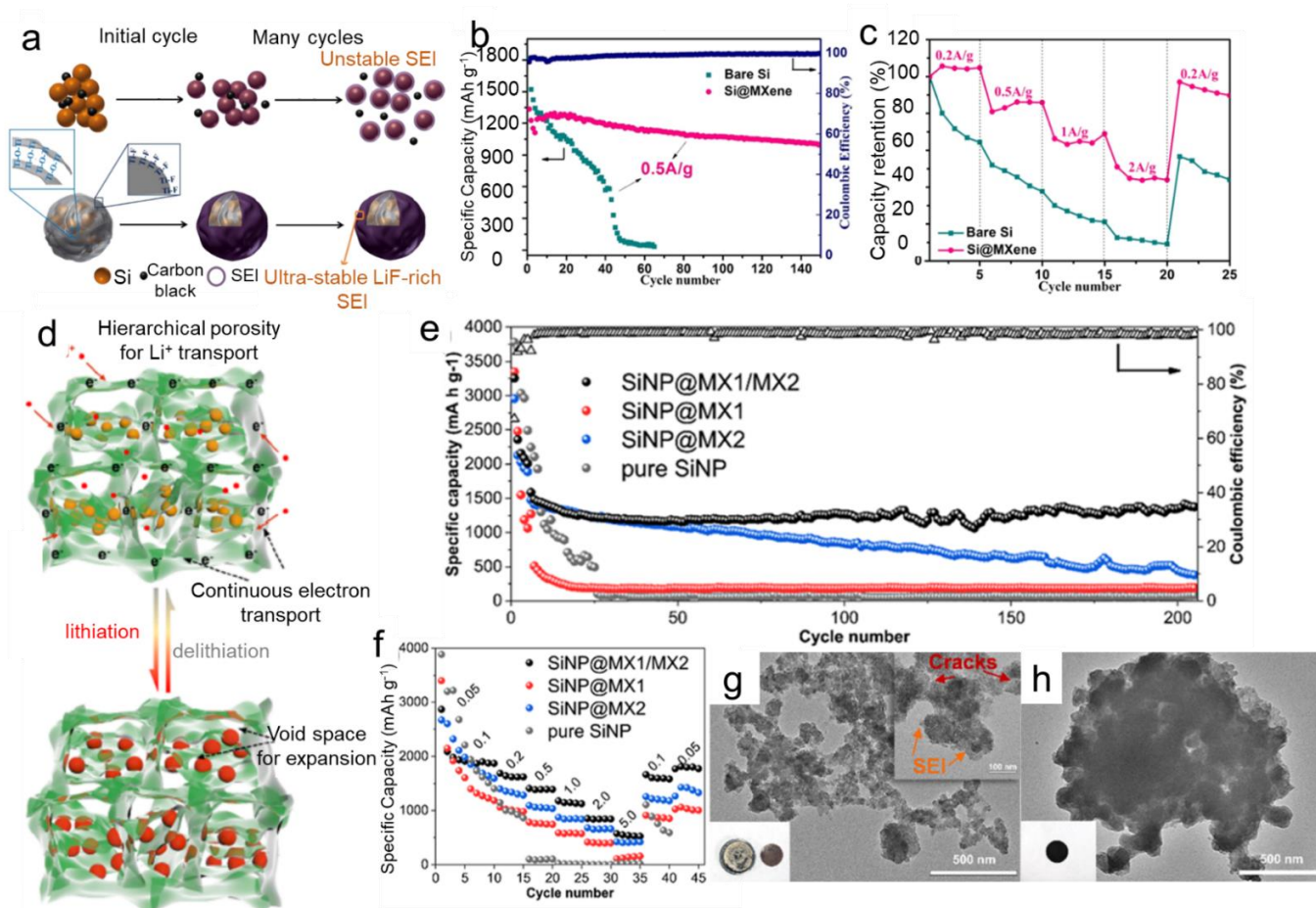


Figure 11. (a) Schematic illustration of Si-based negatodes with and without the protective MXene shell during cycling. (b) Cycling and (c) rate performances of Si negatodes with and without the protective MXene shell at 0.5 A g^{-1} . (d) Schemes of reversible volume change, Li^+ ions, and electronic conduction paths in the SiNP@MXene1/MXene2 negatode during lithiation and delithiation. (e) Long-term cycling performance at 0.5 A g^{-1} . (f) Rate capability at various specific currents. (g,h) TEM images of cycled SiNP and SiNP@MXene1/MXene2, respectively. (Reprinted with permission from Ref. [65], Copyright 2020 ACS Publishers; reprinted with permission from Ref. [59], Copyright 2020 ACS Publishers, respectively).

The above-mentioned 3D porous structure composites of Si@MXene1/MXene2 reported by Li et al. possess two benefits of the stabilized SEI layer by coating and 3D porous structures [59]. Figure 11d shows the transfer route of the Li^+ ion and the alloying reaction process between Li^+ ion and silicon during the charge and discharge process. It can be seen that the volume expansion of silicon during lithiation would not cause the transformation of the entire composite structure, nor would it cause the separation of SiNPs from the 3D MXene framework, resulting from the dual-MXene utilization in this composite. The wrapped MXene1 layer could help to form a more stable SEI film as is the case in Figure 11a, while the porous MXene2 frame could provide large space for the expansion of silicon and high specific surface area as well as the channel for electron and Li^+ ion to transfer. The synergistic effect of Si, MXene1, and MXene2 optimized the electrochemical performance of the composites as shown in Figure 11e,f. Furthermore, Si@MXene1/MXene2 provided the highest discharge capacity of 1422 mAh g^{-1} at 0.5 A g^{-1} after 200 cycles, higher than the pure silicon and single-MXene/Si composites, implying the insufficient protection of single

MXene. Si@MXene1/MXene2 also exhibited high rate capability, whose charge capacity remained 852 and 574 mA g⁻¹ at the high specific currents of 2 and 5 A g⁻¹. The micro-morphology of Si and Si@MXene1/MXene2 after 200 cycles can be found in Figure 11g,h, respectively. Pure silicon exhibited cracks and silicon particles were embedded by the thick SEI film. The Si@MXene1/MXene2 still presented an integrated 3D porous structure after cycling, indicating the high stability of the dual-MXene structure.

Introducing the third component into Si/MXene composites could improve the electro-chemical performance of Si/MXene negatodes, such as carbon and SiO_x. Using N-doped carbon (NC) to wrap the SiNPs in Si/MXene composites, Jo et al. presented improved Li storage properties [57]. In Figures 11 and 12a, Si@NC/MXene demonstrate higher discharge capacities of 953 mAh g⁻¹ after 300 cycles at 0.1 A g⁻¹ due to the incorporation of MXene and NC into SiNPs. Interestingly, Si@NC/MXene also presented superior rate capability with the reversible capacities of 1200 and 849 mAh g⁻¹ at 5 and 10 A g⁻¹, respectively (Figures 11 and 12b). Therefore, the introduction of MXene and N-doped carbon could considerably enhance the rate performance and stability of Si@NC/MXene.

By the co-introduction of SiO_x and carbon into Si/MXene in one step, the layer-by-layer structured MXene/Si@SiO_x@C exhibited excellent structural stability and, as a result, along cycling performance [48]. Figure 12c compares the cycling performance of Si/C with three types of MXene/Si@SiO_x@C composites with different weight ratios at 0.2 C for 200 cycles. As can be seen, MXene/Si@SiO_x@C-2 with approximately 16.9% MXene delivered a reversible capacity of 1547 mAh g⁻¹ and a coulombic efficiency of nearly 100%, which is evidently higher than that of Si/C (238 mAh g⁻¹) and the other two composites with MXene ratio of 10.7% (1049 mAh g⁻¹) and 25.6% (1226 mAh g⁻¹). They also carried out a much longer cycling test at a high rate of 10 C with the optimal composite and achieved a stable capacity of greater than 500 mAh g⁻¹. The soft package full cell had also been prepared with NCM622 as the positive electrode to evaluate the applicability of MXene/Si@SiO_x@C, as shown in Figure 12e. The corresponding reaction equation is as follows [48]:



As shown in Figure 12f, it presented high capacities of 181, 175, and 171 mAh g⁻¹ at the first, 100th, and 200th with superior cyclic stability.

In the sandwiched structure on single layer MXene nanosheets, named as Ti₃C₂@Si/SiO_x@TiO₂, the co-introduction of amorphous SiO_x and TiO₂ layer on the surface of SiNPs could also assist in the formation of stable SEI film (Figure 12g) [61]. Both the amorphous SiO_x and TiO₂ layers should offer some capacity for lithium storage. Due to the lithiation characteristics of SiO_x, the volume change would be smaller than that of silicon. Considering the higher flexibility of SiO_x, it could alleviate the volume expansion of silicon. The high mechanical and chemical stability of TiO₂ means that it could separate the silicon and electrolyte to construct a more stable SEI layer. The Ti₃C₂ nanosheets worked as high-conductive carriers and matrices to hold the SiNPs, which provide a large Li storage capacity. In Figure 12h, the cyclic performance of composites with and without an amorphous TiO₂ layer were compared at 100 and 1000 mAh g⁻¹ for 250 cycles, and Ti₃C₂@Si/SiO_x@TiO₂ exhibited higher capacities and retention rates.

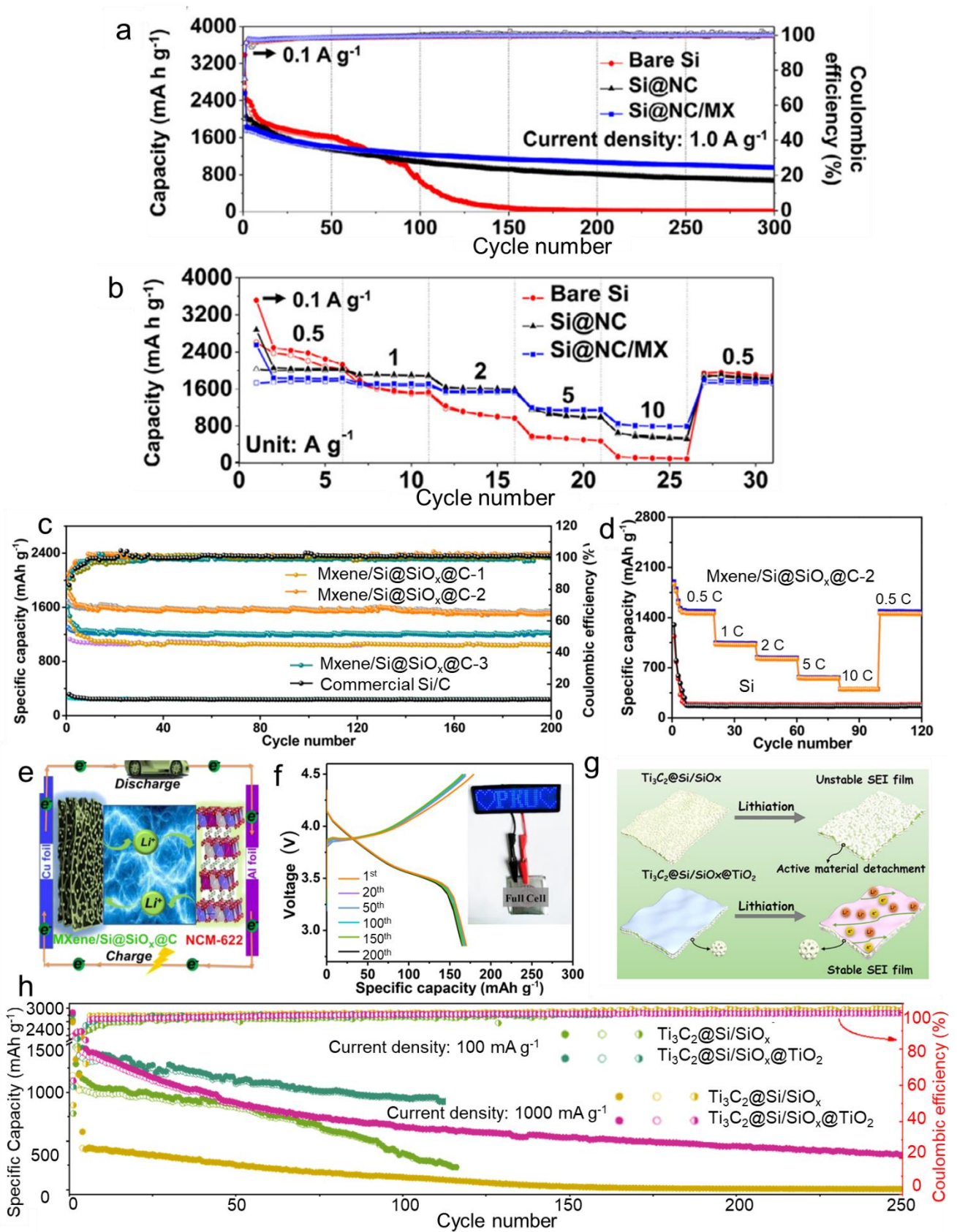


Figure 12. (a) Cycling stability and (b) rate capability of the electrodes based on bare Si, Si@NC, and Si@NC/MXene composites. (Reprinted with permission from Ref. [57], Copyright 2021 Elsevier). (c) Cycling performance of MXene/Si@SiO_x@C-1, MXene/Si@SiO_x@C-2, MXene/Si@SiO_x@C-3 and

bare Si electrodes at 0.2 C for 200 cycles. (d) The charge/discharge profiles of MXene/Si@SiO_x@C-2 electrode at different current rates. (e) Schematic of the configuration of an MXene/Si@SiO_x@C//Li[Ni_{0.6}Co_{0.2}Mn_{0.2}]O₂ full battery. (f) Charge/discharge curves of Al-plastic film soft package Li⁺ ion full battery (inset) with MXene/Si@SiO_x@C-2//Li[Ni_{0.6}Co_{0.2}Mn_{0.2}]O₂ at 0.2 C. (g) Schematic of lithiation process of Ti₃C₂@Si/SiO_x@TiO₂. (h) Cycling performances of Ti₃C₂@Si/SiO_x@TiO₂ and Ti₃C₂@Si/SiO_x at different current densities. (Reprinted with permission from Ref. [48], Copyright 2019 ACS Publishers; reprinted with permission from Ref. [61], Copyright 2020 ACS Publishers, respectively).

4. Conclusions and Perspective

Lithium ion batteries (LIBs) represent possibly the most important energy storage technology, and have been investigated thoroughly in the past several decades to meet the market demand for energy storage in, for example, electric vehicles and power grids. Current commercial LIBs still face technological and market calls for increased energy capacity and service life. Silicon is widely recognized for its very high theoretical lithium storage capacity, appropriate lithiation potential range, and abundant natural resources, which proves promising for the next generation of negative materials in LIBs. However, silicon has a low conductivity, experiences huge volume expansion and becomes structurally unstable upon lithiation, making it unsuitable for practical uses. Construction of composite structures is an important strategy to maintain the structural integrity and improve the stability and electric conductivity of silicon negative electrodes. In the past decade, many novel 2D transition-metal carbides termed as MXenes have been developed and investigated because of their interesting and desirable structural, electric, electrochemical, and mechanical properties [77]. For energy storage applications, MXenes have attracted increasing attention because, for example, they can incorporate silicon nanoparticles (SiNPs) into their layered structures and form various composites, i.e., Si/MXenes, such as Si/Ti₃C₂T_x which is the focus in this article, leading to significantly improved negative performance in LIBs. Such an improvement is, at least partly, attributable to surface functional groups such as -O, -OH, and/or -F in MXenes being prone to bonding with silicon, decreasing the reaction probability with electrolytes.

According to methods of synthesis and structures, Si/MXene composites (Si/Ti₃C₂T_x) can be classified into the following four categories: layer-by-layer assemblies, porous 3D frameworks, self-standing films, and coatings. The synthesis of Si/MXenes can be achieved via common laboratory methods, including mechanical or ball milling mixing, wet processing, spray drying, magnesiothermic reduction, vacuum-assisted filtration, and freeze-drying. Nonetheless, Si/MXene composites prepared in such a way may not always perform to expectation in LIBs, and require further improvement. Modification of the interface between silicon and MXene could effectively strengthen the interactions between silicon and MXene nanosheets and control the surface reaction of silicon. An effective approach is surface functionalization to form positively charged SiNPs and to permit more effective electrostatic attraction with the negatively charged MXene due to their surface terminal groups. For instance, pure SiNPs decays rapidly from the original 3781 to 81 mAh g⁻¹, but the hierarchical SiNPs/MXene (Ti₃C₂T_x) composites delivered a high capacity of 1422 mAh g⁻¹ at 0.5 A g⁻¹ after 200 cycles, indicating excellent discharge capacity retention [59].

Until now, titanium-carbide-based MXenes are mainly synthesized by HF or HCl-LiF etching of the respective MAX phase materials, e.g., Ti₃AlC₂ to Ti₃C₂T_x. The main challenges are to develop more effective exfoliation techniques to make thinner MXene nanosheets and to prepare large-scale single-layered MXenes for mass application [43,78]. In addition, the environmental impact of exfoliation by chemical agents should be taken into consideration. The utilization of fluoride-based etchants would bring surface functional groups such as -O, -OH, and/or -F, which are prone to bonding with silicon, but also react with electrolytes and decrease the initial coulombic efficiency (ICE). Therefore, the

precise control of surface functional groups and hence the chemical and thermal stabilities of MXenes should be further investigated for practical application.

The design of Si/MXene ($\text{Ti}_3\text{C}_2\text{T}_x$) composite structures should consider the contact between SiNPs and MXene nanosheets and the formation of void spaces which can provide room to accommodate for the volume expansion and shrinkage of silicon. Introducing other new materials and constructing hierarchical structures of Si/MXene composites could be conducted to obtain better electrochemical properties such as long cycle life, high cyclic, and rate capacities.

The low ICE is one of the great challenges for Si-based negatodes, which results mainly from the irreversible capacity loss and unstable SEI layer formed in the first cycle. Developing new electrolytes compatible with Si/MXene ($\text{Ti}_3\text{C}_2\text{T}_x$) composites, surface coating to silicon with MXene or other materials, and prelithiation can improve the stability of the SEI layer and hence improve the ICE of Si-based composites. Besides, compatible electrolyte and strong bonding with silicon could both help to maintain the stability of MXene and to inhibit reactions between surface functional groups and electrolyte.

Binder optimization is another important strategy for stabilizing Si-based negatodes. By combining the silicon material with advanced binders, an enhanced adhesion between the Si and binder can be obtained by an integral design. As for the self-standing Si/MXene film, MXene ($\text{Ti}_3\text{C}_2\text{T}_x$) nanosheets can act as both multifunctional binder and matrix to assemble binder-free LIBs. In addition, such a free-standing integrated electrodes can also be utilized for the further application of flexible cells in wearable devices. Combining the advantages of MXene materials, composite structure, as well as the appropriate binder and electrolyte, the stability of Si-based electrodes could be considerably improved.

Although they present many promising properties, Si/MXenes ($\text{Ti}_3\text{C}_2\text{T}_x$) composite negatodes are still in their preliminary stages of research and development. For academic research, the delicate design of a stable composite structure and the electrochemical reaction process should be investigated, including the electrochemical reaction mechanism for Si/MXene composites, especially during SEI film formation, which may require combination with in situ techniques. For industrial production, there are several issues to be solved. The production process should be scalable, consistent, and easy to operate. Cost and yield are also key aspects for the commercialization of Si/MXene. The cost of raw materials and the complex preparation of Si/MXene materials should be further considered.

Author Contributions: Conceptualization, T.J. and G.Z.C.; methodology, T.J. and H.Y.; investigation, T.J., H.Y. and G.Z.C.; resources, T.J.; writing—original draft preparation, T.J. and H.Y.; writing—review and editing, T.J. and G.Z.C.; visualization, T.J. and G.Z.C.; supervision, T.J. and G.Z.C.; project administration, T.J.; funding acquisition, T.J. All authors have read and agreed to the published version of the manuscript.

Funding: This research was funded by Natural Science Foundation of Hubei Province (grant number: 2021CFB434) and National Natural Science Foundation of China (grant number: 51602234).

Conflicts of Interest: The authors declare no conflict of interest.

References

1. Wang, F.; Wu, X.; Li, C.; Zhu, Y.; Fu, L.; Wu, Y.; Liu, X. Nanostructured positive electrode materials for post-lithium ion batteries. *Energy Environ. Sci.* **2016**, *9*, 3570–3611. [[CrossRef](#)]
2. Han, G.-B.; Ryou, M.-H.; Cho, K.Y.; Lee, Y.M.; Park, J.-K. Effect of succinic anhydride as an electrolyte additive on electrochemical characteristics of silicon thin-film electrode. *J. Power Sources* **2010**, *195*, 3709–3714. [[CrossRef](#)]
3. Wang, T.; Ji, X.; Wu, F.; Yang, W.; Dai, X.; Xu, X.; Wang, J.; Guo, D.; Chen, M. Facile fabrication of a three-dimensional coral-like silicon nanostructure coated with a C/rGO double layer by using the magnesiothermic reduction of silica nanotubes for high-performance lithium-ion battery anodes. *J. Alloys Compd.* **2021**, *863*, 158569. [[CrossRef](#)]
4. Huang, S.; Qin, X.; Lei, C.; Miao, X.; Wei, T. A one-pot method to fabricate reduced graphene oxide (rGO)-coated $\text{Si@SiO}_x/\beta\text{-Bi}_2\text{O}_3/\text{Bi}$ composites for lithium-ion batteries. *Electrochim. Acta* **2021**, *390*, 138857. [[CrossRef](#)]
5. Lu, Q.; Jeong, B.-G.; Peng, X.; Jeong, S.-W.; Xie, B.; Wu, Z. The robust carbon shell to improve stability of porous Si anodes for high-performance lithium-ion batteries. *J. Alloys Compd.* **2021**, *877*, 160193. [[CrossRef](#)]

6. Liu, X.H.; Liu, Y.; Kushima, A.; Zhang, S.; Zhu, T.; Li, J.; Huang, J.Y. In Situ TEM Experiments of Electrochemical Lithiation and Delithiation of Individual Nanostructures. *Adv. Energy Mater.* **2012**, *2*, 722–741. [[CrossRef](#)]
7. McDowell, M.T.; Lee, S.W.; Nix, W.D.; Cui, Y. 25th anniversary article: Understanding the lithiation of silicon and other alloying anodes for lithium-ion batteries. *Adv. Mater.* **2013**, *25*, 4966–4985. [[CrossRef](#)]
8. Obrovac, M.N.; Krause, L.J. Reversible Cycling of Crystalline Silicon Powder. *J. Electrochem. Soc.* **2007**, *154*, A103–A108. [[CrossRef](#)]
9. Rhodes, K.; Dudney, N.; Lara-Curzio, E.; Daniel, C. Understanding the Degradation of Silicon Electrodes for Lithium-Ion Batteries Using Acoustic Emission. *J. Electrochem. Soc.* **2010**, *157*, A1354–A1360. [[CrossRef](#)]
10. Ryu, J.; Chen, T.; Bok, T.; Song, G.; Ma, J.; Hwang, C.; Luo, L.; Song, H.K.; Cho, J.; Wang, C.; et al. Mechanical mismatch-driven rippling in carbon-coated silicon sheets for stress-resilient battery anodes. *Nat. Commun.* **2018**, *9*, 2924. [[CrossRef](#)] [[PubMed](#)]
11. Guo, Y.-G.; Hu, J.-S.; Wan, L.-J. Nanostructured Materials for Electrochemical Energy Conversion and Storage Devices. *Adv. Mater.* **2008**, *20*, 2878–2887. [[CrossRef](#)]
12. Kwon, H.J.; Hwang, J.Y.; Shin, H.J.; Jeong, M.G.; Chung, K.Y.; Sun, Y.K.; Jung, H.G. Nano/Microstructured Silicon-Carbon Hybrid Composite Particles Fabricated with Corn Starch Biowaste as Anode Materials for Li-Ion Batteries. *Nano Lett.* **2020**, *20*, 625–635. [[CrossRef](#)]
13. Jin, H.; Zhu, M.; Liu, J.; Gan, L.; Gong, Z.; Long, M. Alkaline chitosan solution as etching phase to design Si@SiO₂@N-Carbon anode for Lithium-ion battery. *Appl. Surf. Sci.* **2021**, *541*, 148436. [[CrossRef](#)]
14. Zhou, X.; Xie, H.; He, X.; Zhao, Z.; Ma, Q.; Cai, M.; Yin, H. Annihilating the Formation of Silicon Carbide: Molten Salt Electrolysis of Carbon-Silica Composite to Prepare the Carbon-Silicon Hybrid for Lithium-Ion Battery Anode. *Energy Environ. Mater.* **2020**, *3*, 166–176. [[CrossRef](#)]
15. Zhang, J.; Hou, Z.; Zhang, X.; Zhang, L.; Li, C. Delicate construction of Si@SiO_x composite materials by microwave hydrothermal for lithium-ion battery anodes. *Ionics* **2019**, *26*, 69–74. [[CrossRef](#)]
16. Guo, J.; Zhai, W.; Sun, Q.; Ai, Q.; Li, J.; Cheng, J.; Dai, L.; Ci, L. Facilely tunable core-shell Si@SiO_x nanostructures prepared in aqueous solution for lithium ion battery anode. *Electrochim. Acta* **2020**, *342*, 136068. [[CrossRef](#)]
17. Chen, Q.; Tan, L.; Wang, S.; Liu, B.; Peng, Q.; Luo, H.; Jiang, P.; Tang, H.; Sun, R. A facile synthesis of phosphorus doped Si/SiO₂/C with high coulombic efficiency and good stability as an anode material for lithium ion batteries. *Electrochim. Acta* **2021**, *385*, 138385. [[CrossRef](#)]
18. Wu, J.; Liu, J.; Wang, Z.; Gong, X.; Wang, Y. A new design for Si wears double jackets used as a high-performance lithium-ion battery anode. *Chem. Eng. J.* **2019**, *370*, 565–572. [[CrossRef](#)]
19. Xiang, J.; Liu, H.; Na, R.; Wang, D.; Shan, Z.; Tian, J. Facile preparation of void-buffered Si@TiO₂/C microspheres for high-capacity lithium ion battery anodes. *Electrochim. Acta* **2020**, *337*, 135841. [[CrossRef](#)]
20. Yang, Y.; Yang, H.-R.; Seo, H.; Kim, K.; Kim, J.-H. Novel synthesis of porous Si-TiO₂ composite as a high-capacity anode material for Li secondary batteries. *J. Alloys Compd.* **2021**, *872*, 159640. [[CrossRef](#)]
21. Cai, X.; Lai, L.; Shen, Z.; Lin, J. Graphene and graphene-based composites as Li-ion battery electrode materials and their application in full cells. *J. Mater. Chem. A* **2017**, *5*, 15423–15446. [[CrossRef](#)]
22. Wang, D.; Guo, G.-C.; Wei, X.-L.; Liu, L.-M.; Zhao, S.-J. Phosphorene ribbons as anode materials with superhigh rate and large capacity for Li-ion batteries. *J. Power Sources* **2016**, *302*, 215–222. [[CrossRef](#)]
23. Naresh, K.J.; Rafael, B.A.; Vivekanand, S.; Rajeev, A. Borophane as a Bench-mate of Graphene: A Potential 2D Material for Anode of Li and Na-ion Batteries. *ACS Appl. Mater. Interfaces* **2017**, *9*, 16148–16158.
24. Zhao, G.; Cheng, Y.; Sun, P.; Ma, W.; Hao, S.; Wang, X.; Xu, X.; Xu, Q.; Liu, M. Biocarbon based template synthesis of uniform lamellar MoS₂ nanoflowers with excellent energy storage performance in lithium-ion battery and supercapacitors. *Electrochim. Acta* **2020**, *331*, 135262. [[CrossRef](#)]
25. Folorunso, O.; Kumar, N.; Hamam, Y.; Sadiku, R.; Ray, S.S. Recent progress on 2D metal carbide/nitride (MXene) nanocomposites for lithium-based batteries. *FlatChem* **2021**, *29*, 100281. [[CrossRef](#)]
26. Du, L.; Lin, H.; Ma, Z.; Wang, Q.; Li, D.; Shen, Y.; Zhang, W.; Rui, K.; Zhu, J.; Huang, W. Using and recycling V₂O₅ as high performance anode materials for sustainable lithium ion battery. *J. Power Sources* **2019**, *424*, 158–164. [[CrossRef](#)]
27. Yang, J.; Liu, J.; Zhao, C.; Zhang, W.; Li, X. Core-shell structured heterohierarchical porous Si@graphene microsphere for high-performance lithium-ion battery anodes. *Mater. Lett.* **2020**, *266*, 127484. [[CrossRef](#)]
28. Han, X.; Zhang, Z.; Chen, H.; Zhang, Q.; Chen, S.; Yang, Y. On the Interface Design of Si and Multilayer Graphene for a High-Performance Li-Ion Battery Anode. *ACS Appl. Mater. Interfaces* **2020**, *12*, 44840–44849. [[CrossRef](#)]
29. Yang, Y.; Yang, H.-X.; Wu, Y.-Q.; Pu, H.; Meng, W.-J.; Gao, R.-Z.; Zhao, D.-L. Graphene caging core-shell Si@Cu nanoparticles anchored on graphene sheets for lithium-ion battery anode with enhanced reversible capacity and cyclic performance. *Electrochim. Acta* **2020**, *341*, 136037. [[CrossRef](#)]
30. Srimuk, P.; Kaasik, F.; Krüner, B.; Tolosa, A.; Fleischmann, S.; Jäckel, N.; Tekeli, M.C.; Aslan, M.; Suss, M.E.; Presser, V. MXene as a novel intercalation-type pseudocapacitive cathode and anode for capacitive deionization. *J. Mater. Chem. A* **2016**, *4*, 18265–18271. [[CrossRef](#)]
31. Li, D.; Chen, X.; Xiang, P.; Du, H.; Xiao, B. Chalcogenated-Ti₃C₂X₂ MXene (X = O, S, Se and Te) as a high-performance anode material for Li-ion batteries. *Appl. Surf. Sci.* **2020**, *501*, 144221. [[CrossRef](#)]
32. Wang, Z.; Xu, Z.; Huang, H.; Chu, X.; Xie, Y.; Xiong, D.; Yan, C.; Zhao, H.; Zhang, H.; Yang, W. Unraveling and Regulating Self-Discharge Behavior of Ti₃C₂T_x MXene-Based Supercapacitors. *ACS Nano* **2020**, *14*, 4916–4924. [[CrossRef](#)] [[PubMed](#)]

33. Yun, T.; Kim, H.; Iqbal, A.; Cho, Y.S.; Lee, G.S.; Kim, M.K.; Kim, S.J.; Kim, D.; Gogotsi, Y.; Kim, S.O.; et al. Electromagnetic Shielding of Monolayer MXene Assemblies. *Adv. Mater.* **2020**, *32*, 1906769. [[CrossRef](#)] [[PubMed](#)]
34. Wang, H.; Lee, J.-M. Recent advances in structural engineering of MXene electrocatalysts. *J. Mater. Chem. A* **2020**, *8*, 10604–10624. [[CrossRef](#)]
35. Lei, J.-C.; Zhang, X.; Zhou, Z. Recent advances in MXene: Preparation, properties, and applications. *Front. Phys.* **2015**, *10*, 276–286. [[CrossRef](#)]
36. Huang, S.; Mutyala, K.C.; Sumant, A.V.; Mochalin, V.N. Achieving superlubricity with 2D transition metal carbides (MXenes) and MXene/graphene coatings. *Mater. Today Adv.* **2021**, *9*, 100133. [[CrossRef](#)]
37. Han, X.; Zhou, W.; Chen, M.; Chen, J.; Wang, G.; Liu, B.; Luo, L.; Chen, S.; Zhang, Q.; Shi, S.; et al. Interfacial nitrogen engineering of robust silicon/MXene anode toward high energy solid-state lithium-ion batteries. *J. Energy Chem.* **2022**, *67*, 727–735. [[CrossRef](#)]
38. Gou, L.; Jing, W.; Li, Y.; Wang, M.; Hu, S.; Wang, H.; He, Y.-B. Lattice-Coupled Si/MXene Confined by Hard Carbon for Fast Sodium-Ion Conduction. *ACS Appl. Energy Mater.* **2021**, *4*, 7268–7277. [[CrossRef](#)]
39. Ahmed, B.; Anjum, D.H.; Gogotsi, Y.; Alshareef, H.N. Atomic layer deposition of SnO₂ on MXene for Li-ion battery anodes. *Nano Energy* **2017**, *34*, 249–256. [[CrossRef](#)]
40. Chen, C.; Xie, X.; Anasori, B.; Sarycheva, A.; Makaryan, T.; Zhao, M.; Urbankowski, P.; Miao, L.; Jiang, J.; Gogotsi, Y. MoS₂-on-MXene Heterostructures as Highly Reversible Anode Materials for Lithium-Ion Batteries. *Angew. Chem. Int. Ed. Engl.* **2018**, *57*, 1846–1850. [[CrossRef](#)]
41. Cui, Y.; Wang, J.; Wang, X.; Qin, J.; Cao, M. A Hybrid Assembly of MXene with NH₂-Si Nanoparticles Boosting Lithium Storage Performance. *Chem. Asian J.* **2020**, *15*, 1376–1383. [[CrossRef](#)] [[PubMed](#)]
42. Luo, J.; Matios, E.; Wang, H.; Tao, X.; Li, W. Interfacial structure design of MXene-based nanomaterials for electrochemical energy storage and conversion. *InfoMat* **2020**, *2*, 1057–1076. [[CrossRef](#)]
43. Naguib, M.; Kurtoglu, M.; Presser, V.; Lu, J.; Niu, J.; Heon, M.; Hultman, L.; Gogotsi, Y.; Barsoum, M.W. Two-dimensional nanocrystals produced by exfoliation of Ti₃AlC₂. *Adv. Mater.* **2011**, *23*, 4248–4253. [[CrossRef](#)] [[PubMed](#)]
44. Xiao, H.L.; Li, Z.; Shan, H.; Scott, X.M.; Ting, Z.; Jian, Y.H. Size-Dependent Fracture of Silicon Nanoparticles During Lithiation. *ACS Nano* **2012**, *6*, 1522–1531.
45. Zhang, F.; Jia, Z.; Wang, C.; Feng, A.; Wang, K.; Hou, T.; Liu, J.; Zhang, Y.; Wu, G. Sandwich-like silicon/Ti₃C₂T_x MXene composite by electrostatic self-assembly for high performance lithium ion battery. *Energy* **2020**, *195*, 117047. [[CrossRef](#)]
46. Zhu, X.; Shen, J.; Chen, X.; Li, Y.; Peng, W.; Zhang, G.; Zhang, F.; Fan, X. Enhanced cycling performance of Si-MXene nanohybrids as anode for high performance lithium ion batteries. *Chem. Eng. J.* **2019**, *378*, 122212. [[CrossRef](#)]
47. Kong, F.; He, X.; Liu, Q.; Qi, X.; Sun, D.; Zheng, Y.; Wang, R.; Bai, Y. Enhanced reversible Li-ion storage in Si@Ti₃C₂ MXene nanocomposite. *Electrochem. Commun.* **2018**, *97*, 16–21. [[CrossRef](#)]
48. Zhang, Y.; Mu, Z.; Lai, J.; Chao, Y.; Yang, Y.; Zhou, P.; Li, Y.; Yang, W.; Xia, Z.; Guo, S. MXene/Si@SiO_x@C Layer-by-Layer Superstructure with Autoadjustable Function for Superior Stable Lithium Storage. *ACS Nano* **2019**, *13*, 2167–2175. [[CrossRef](#)] [[PubMed](#)]
49. Zhang, C.J.; Park, S.-H.; Seral-Ascaso, A.; Barwich, S.; McEvoy, N.; Boland, C.S.; Coleman, J.N.; Gogotsi, Y.; Nicolosi, V. High capacity silicon anodes enabled by MXene viscous aqueous ink. *Nat. Commun.* **2019**, *10*, 849. [[CrossRef](#)]
50. Yang, Q.; Wang, Z.; Xia, Y.; Wu, G.; Chen, C.; Wang, J.; Rao, P.; Dong, A. Facile electrostatic assembly of Si@MXene superstructures for enhanced lithium-ion storage. *J. Colloid Interface Sci.* **2020**, *580*, 68–76. [[CrossRef](#)] [[PubMed](#)]
51. An, Y.; Tian, Y.; Zhang, Y.; Wei, C.; Tan, L.; Zhang, C.; Cui, N.; Xiong, S.; Feng, J.; Qian, Y. Two-Dimensional Silicon/Carbon from Commercial Alloy and CO₂ for Lithium Storage and Flexible Ti₃C₂T_x MXene-Based Lithium-Metal Batteries. *ACS Nano* **2020**, *14*, 17574–17588. [[CrossRef](#)] [[PubMed](#)]
52. Li, H.; Lu, M.; Han, W.; Li, H.; Wu, Y.; Zhang, W.; Wang, J.; Zhang, B. Employing MXene as a matrix for loading amorphous Si generated upon lithiation towards enhanced lithium-ion storage. *J. Energy Chem.* **2019**, *38*, 50–54. [[CrossRef](#)]
53. Zhang, P.; Zhu, Q.; Guan, Z.; Zhao, Q.; Sun, N.; Xu, B. A Flexible Si@C Electrode with Excellent Stability Employing an MXene as a Multifunctional Binder for Lithium-Ion Batteries. *ChemSusChem* **2020**, *13*, 1621–1628. [[CrossRef](#)]
54. Tian, Y.; An, Y.; Feng, J. Flexible and Freestanding Silicon/MXene Composite Papers for High-Performance Lithium-Ion Batteries. *ACS Appl. Mater. Interfaces* **2019**, *11*, 10004–10011. [[CrossRef](#)] [[PubMed](#)]
55. Cao, D.; Ren, M.; Xiong, J.; Pan, L.; Wang, Y.; Ji, X.; Qiu, T.; Yang, J.; Zhang, C. Self-assembly of hierarchical Ti₃C₂T_x-CNT/SiNPs resilient films for high performance lithium ion battery electrodes. *Electrochim. Acta* **2020**, *348*, 136211. [[CrossRef](#)]
56. Hui, X.; Zhao, R.; Zhang, P.; Li, C.; Wang, C.; Yin, L. Low-Temperature Reduction Strategy Synthesized Si/Ti₃C₂ MXene Composite Anodes for High-Performance Li-Ion Batteries. *Adv. Energy Mater.* **2019**, *9*, 1901065. [[CrossRef](#)]
57. Jo, D.Y.; Kim, J.K.; Oh, H.G.; Kang, Y.C.; Park, S.-K. Chemically Integrating MXene Nanosheets with N-Doped C-Coated Si Nanoparticles for Enhanced Li Storage Performance. *Scr. Mater.* **2021**, *199*, 113840. [[CrossRef](#)]
58. Wang, Z.; Cao, D.; Ren, M.; Zhang, H.; Pan, L.; John Zhang, C.; Yang, J. Si@Ti₃C₂T_x with Si nanoparticles embedded in a 3D conductive network of crumpled Ti₃C₂T_x nanosheets for the anode of lithium-ion batteries with enhanced cycling performance. *J. Alloys Compd.* **2022**, *892*, 162037. [[CrossRef](#)]
59. Li, X.; Chen, Z.; Li, A.; Yu, Y.; Chen, X.; Song, H. Three-Dimensional Hierarchical Porous Structures Constructed by Two-Stage MXene-Wrapped Si Nanoparticles for Li-Ion Batteries. *ACS Appl. Mater. Interfaces* **2020**, *12*, 48718–48728. [[CrossRef](#)]

60. Liu, S.; Zhang, X.; Yan, P.; Cheng, R.; Tang, Y.; Cui, M.; Wang, B.; Zhang, L.; Wang, X.; Jiang, Y.; et al. Dual Bond Enhanced Multidimensional Constructed Composite Silicon Anode for High-Performance Lithium Ion Batteries. *ACS Nano* **2019**, *13*, 8854–8864. [[CrossRef](#)] [[PubMed](#)]
61. Jiang, M.; Zhang, F.; Zhu, G.; Ma, Y.; Luo, W.; Zhou, T.; Yang, J. Interface-Amorphized $\text{Ti}_3\text{C}_2\text{@Si/SiO}_x\text{@TiO}_2$ Anodes with Sandwiched Structures and Stable Lithium Storage. *ACS Appl. Mater. Interfaces* **2020**, *12*, 24796–24805. [[CrossRef](#)] [[PubMed](#)]
62. Jiang, M.; Jiang, M.; Gao, H.; Chen, J.; Liu, W.; Ma, Y.; Luo, W.; Yang, J. Comparison of Additives in Anode: The Case of Graphene, MXene, CNTs Integration with Silicon Inside Carbon Nanofibers. *Acta Metall. Sin. Engl. Lett.* **2020**, *34*, 337–346. [[CrossRef](#)]
63. Meng, J.; Zhang, F.; Zhang, L.; Liu, L.; Chen, J.; Yang, B.; Yan, X. Rolling up MXene sheets into scrolls to promote their anode performance in lithium-ion batteries. *J. Energy Chem.* **2020**, *46*, 256–263. [[CrossRef](#)]
64. Xia, M.; Chen, B.; Gu, F.; Zu, L.; Xu, M.; Feng, Y.; Wang, Z.; Zhang, H.; Zhang, C.; Yang, J. $\text{Ti}_3\text{C}_2\text{T}_x$ MXene Nanosheets as a Robust and Conductive Tight on Si Anodes Significantly Enhance Electrochemical Lithium Storage Performance. *ACS Nano* **2020**, *14*, 5111–5120. [[CrossRef](#)]
65. Yan, Y.; Zhao, X.; Dou, H.; Wei, J.; Sun, Z.; He, Y.S.; Dong, Q.; Xu, H.; Yang, X. MXene Frameworks Promote the Growth and Stability of LiF-Rich Solid-Electrolyte Interphases on Silicon Nanoparticle Bundles. *ACS Appl. Mater. Interfaces* **2020**, *12*, 18541–18550. [[CrossRef](#)]
66. Zhou, H.; Cui, C.; Cheng, R.; Yang, J.; Wang, X. MXene Enables Stable Solid-Electrolyte Interphase for Si@MXene Composite with Enhanced Cycling Stability. *ChemElectroChem* **2021**, *8*, 3089–3094. [[CrossRef](#)]
67. Yan, Y.; He, Y.-S.; Zhao, X.; Zhao, W.; Ma, Z.-F.; Yang, X. Regulating adhesion of solid-electrolyte interphase to silicon via covalent bonding strategy towards high Coulombic-efficiency anodes. *Nano Energy* **2021**, *84*, 105935. [[CrossRef](#)]
68. Mu, G.; Mu, D.; Wu, B.; Ma, C.; Bi, J.; Zhang, L.; Yang, H.; Wu, F. Microsphere-Like SiO_2 /MXene Hybrid Material Enabling High Performance Anode for Lithium Ion Batteries. *Small* **2020**, *16*, 1905430. [[CrossRef](#)]
69. Mei, S.; Liu, Y.; Fu, J.; Guo, S.; Deng, J.; Peng, X.; Zhang, X.; Gao, B.; Huo, K.; Chu, P.K. Waste-glass-derived silicon/CNTs composite with strong Si-C covalent bonding for advanced anode materials in lithium-ion batteries. *Appl. Surf. Sci.* **2021**, *563*, 150280. [[CrossRef](#)]
70. Tan, Y.; Jiang, T.; Chen, G.Z. Mechanisms and Product Options of Magnesiothermic Reduction of Silica to Silicon for Lithium-Ion Battery Applications. *Front. Energy Res.* **2021**, *9*, 651386. [[CrossRef](#)]
71. Liang, M.; Wang, W.; Jiang, Y.; Liao, C.; Long, Q.; Lai, X.; Liao, L. Fabrication of C@Si@G for flexible lithium-ion batteries. *J. Alloys Compd.* **2021**, *878*, 160357. [[CrossRef](#)]
72. Shao, J.; Yang, Y.; Zhang, X.; Shen, L.; Bao, N. 3D Yolk-Shell Structured Si/void/rGO Free-Standing Electrode for Lithium-Ion Battery. *Materials* **2021**, *14*, 2836. [[CrossRef](#)] [[PubMed](#)]
73. Sun, D.; Wang, M.; Li, Z.; Fan, G.; Fan, L.-Z.; Zhou, A. Two-dimensional Ti_3C_2 as anode material for Li-ion batteries. *Electrochem. Commun.* **2014**, *47*, 80–83. [[CrossRef](#)]
74. Cheng, R.; Hu, T.; Zhang, H.; Wang, C.; Hu, M.; Yang, J.; Cui, C.; Guang, T.; Li, C.; Shi, C.; et al. Understanding the Lithium Storage Mechanism of $\text{Ti}_3\text{C}_2\text{T}_x$ MXene. *J. Phys. Chem. C* **2018**, *123*, 1099–1109. [[CrossRef](#)]
75. Das, P.; Wu, Z.-S. MXene for energy storage: Present status and future perspectives. *J. Phys. Energy* **2020**, *2*, 032004. [[CrossRef](#)]
76. Wei, C.; Fei, H.; Tian, Y.; An, Y.; Tao, Y.; Li, Y.; Feng, J. Scalable construction of SiO /wrinkled MXene composite by a simple electrostatic self-assembly strategy as anode for high-energy lithium-ion batteries. *Chin. Chem. Lett.* **2020**, *31*, 980–983. [[CrossRef](#)]
77. Kshetri, T.; Tran, D.T.; Le, H.T.; Nguyen, D.C.; Hoa, H.V.; Kim, N.H.; Lee, J.H. Recent advances in MXene-based nanocomposites for electrochemical energy storage applications. *Prog. Mater. Sci.* **2021**, *117*, 100733. [[CrossRef](#)]
78. Ghidui, M.; Lukatskaya, M.R.; Zhao, M.Q.; Gogotsi, Y.; Barsoum, M.W. Conductive two-dimensional titanium carbide ‘clay’ with high volumetric capacitance. *Nature* **2014**, *516*, 78–81. [[CrossRef](#)]